Improvements in glycoproteomics through architecture changes to the Orbitrap Tribrid MS platform

Tim S. Veth[1], Emmajay Sutherland[1], Kayla A. Markuson[1], Ruby Zhang[1], Anna G. Duboff[1], Jingjing Huang[2], David Bergen[2], Amanda E. Lee[2], Rafael D. Melani[2], Jesse D. Canterbury[2], Vlad Zabrouskov[2], Graeme C. McAlister[2], Christopher Mullen[2], Nicholas M. Riley[1]*

[1]Department of Chemistry, University of Washington, Seattle, WA, USA
[2]Thermo Fisher Scientific, San Jose, California, USA

†T.S.V. and E.S. contributed equally to this work
*Submit correspondence to nmriley@uw.edu

ABSTRACT
Hardware changes introduced on the Orbitrap Ascend MultiOmics Tribrid MS include dual ion routing multipoles (IRMs) that can enable parallelized accumulation, dissociation, and Orbitrap mass analysis of three separate ion populations. The balance between these instrument functions is especially important in glycoproteomics, where complexities of glycopeptide fragmentation necessitate large precursor ion populations and, consequently, long ion accumulation times for quality MS/MS spectra. To compound matters further, dissociation methods like electron transfer dissociation (ETD) that benefit glycopeptide characterization come with overhead times that also slow down scan acquisition. Here we explored how the dual IRM architecture of the Orbitrap Ascend can improve glycopeptide analysis, with a focus on O-glycopeptide characterization using ETD with supplemental collisional activation (EThcD). We found that parallelization of ion accumulation and EThcD fragmentation – uniquely enabled by the Orbitrap Ascend – increased scan acquisition speed without sacrificing spectral quality, subsequently increasing the number of O-glycopeptides identified relative to analyses on the Orbitrap Eclipse (i.e., the previous generation Tribrid MS). Additionally, we systematically evaluated ion-ion reaction times and supplemental activation energies used for EThcD to understand how best to utilize acquisition time in the dual IRM architecture. We observed that shorter-than-expected ion-ion reaction times minimized scan overhead time without sacrificing c/z•-fragment ion generation, and that higher supplemental collision energies can generate combinations of glycan-retaining and glycan-neutral-loss peptide backbone fragments that benefit O-glycopeptide identification. We also saw improvements in N-glycopeptide analysis using collision-based dissociation, especially with methods using faster scan acquisition speeds. Overall, these data show how architectural changes to the Tribrid MS platform benefit glycoproteomic experiments by parallelizing scan functions to minimize overhead time and improve sensitivity.

KEYWORDS
Glycoproteomics, N-glycopeptides, O-glycopeptides, tandem mass spectrometry, fragmentation, electron transfer dissociation

INTRODUCTION

Glycosylation is a common post-translational modification (PTM) found on nearly 50% of human proteins.[1,2] This PTM plays a fundamental role in biological processes, including cellular communication and recognition, and dysregulation of these processes has been widely implicated in disease.[3–5] Protein glycosylation is highly heterogeneous, with hundreds of glycans resulting from non-templated regulation from approximately 200 glycosyltransferases active in the endoplasmic reticulum and/or Golgi.[6] These glycans can potentially modify tens of thousands of glycosites across the proteome, and glycosites are classified by glycan identity and attachment to amino acid side chains.[7–9] N-glycosylation is defined by an N-glycosidic linkage to asparagine residues within the N-sequon consensus motif (N-X-S/T, where X is any amino acid other than proline).[10–12] O-glycosylation has multiple subclasses, but mucin-type O-glycosylation is arguably the most abundant and involves an initiating N-acetylgalactosamine (GalNAc) attached via an O-glycosidic bond to serine, threonine, and sometimes tyrosine residues.[13–15]

Detailed analysis of precisely what glycans modify specific glycosites is important to understand the functional implications of glycosylation, and mass spectrometry is currently the premier tool for characterizing site-specific glycosylation.[16–18] A typical glycoproteomics workflow entails proteolytic cleavage of glycoproteins followed by analysis of intact glycopeptides via LC-MS/MS,[19] but methods often vary in details involving glycopeptide enrichment,[20,21] data collection,[22,23] and data analysis.[24,25] One important decision in every glycoproteomics experiment is how to maximize the information available in glycopeptide tandem mass spectra, which are the foundation of site-specific analysis.[26–29] Designing methods to maximize both the number of MS/MS spectra acquired and the quality of glycopeptide MS/MS spectra is not trivial, especially on advanced instrumentation that offers multiple fragmentation methods, numerous scan types, and flexible data acquisition schemes.[30–34]

Several instrument platforms have shown promise for flexible glycopeptide characterization, including time-of-flight instruments with ion mobility and multiple ion activation capabilities.[35–39] One popular platform for glycoproteomics is the quadrupole-Orbitrap-linear ion trap Tribrid MS system, which now exists in four distinct generations.[40–43] Flexibility in data acquisition is a hallmark of Orbitrap Tribrid instruments, which is especially useful when designing methods for heterogeneous populations of glycopeptides that may have different analytical needs.[44–46] For example, Orbitrap Tribrids provide multiple modes of peptide activation, including resonant excitation collisional dissociation, beam-type collisional dissociation, electron-driven fragmentation, and photodissociation.[47–54] N-glycoproteomics workflows largely benefit from the acquisition speeds enabled by beam-type collisional activation (called higher-energy collisional dissociation, or HCD, on Orbitrap Tribrids), even though fragment ions often do not retain intact glycans.[55–59] Site-specific characterization of O-glycopeptides, however, requires peptide fragment ions that retain glycan masses, meaning that electron transfer dissociation (ETD) and ETD with supplemental HCD activation (EThcD) are particularly valuable.[59–62] Conveniently, Orbitrap Tribrids enable acquisition schemes that generate MS/MS spectra with varying dissociation types using product-dependent triggering methods and other forms of intelligent data acquisition.[63–66]

Another key feature of Orbitrap Tribrids is the architecture uniting the quadrupole, Orbitrap, and linear ion trap mass analyzers.[40] The first three generations, the Fusion, Fusion Lumos, and Eclipse, built on an architecture with the quadrupole in front of the C-trap and Orbitrap, followed

by an ion routing multipole (IRM), and finally, the linear ion trap (**Figure S1**). This design enables scan parallelization so that two ion populations can be manipulated at once: one being mass analyzed in either the ion trap or Orbitrap while another is accumulated in the IRM for subsequent manipulations.[40] This parallelization has been demonstrated to improve acquisition speeds, especially when combining survey scan acquisition in the Orbitrap with MS/MS scan acquisition in the linear ion trap.[32,41] Using more nuanced scan features, however, such as ETD and EThcD, requires ion manipulations of precursor cations and reagent anions in addition to movement through the IRM prior to mass analysis.[67] These advanced functions create overhead time that can limit parallelization schemes or require balancing scan acquisition speeds at the cost of ion injection time and, ultimately, spectral quality.

The fourth and most recent generation of Orbitrap Tribrid, the Orbitrap Ascend, reimagined the Tribrid architecture by adding a second “front” IRM between the quadrupole and C-trap/Orbitrap to complement the “back” IRM (i.e., the only IRM in previous generations) (**Figure 1A**). Additionally, the Ascend includes redesigned source optics to improve ion transmission and reduce in-source fragmentation, among other engineering improvements to the vacuum system and ion path.[68] Importantly, adding the second IRM enables the manipulation of three ion populations at a time to significantly improve parallelizable ion injection time. This is especially advantageous for methods used in glycoproteomics where overhead time due to scan functions (e.g., ETD) or long accumulation times are unavoidable features.[69] Here we explore how the dual IRM architecture of the Orbitrap Ascend can benefit glycoproteomics data acquisition, especially for O-glycopeptide characterization that requires ETD-based MS/MS scans. Furthermore, we investigate EThcD ion-ion reaction time and supplemental activation energy to understand how to maximize glycopeptide identifications.

EXPERIMENTAL PROCEDURES

Proteins were purchased from R&D Systems (PD-L1, CD80, SARS-CoV-2 spike glycoprotein, CD58, MUC16, CD43, GP1ba, podocalyxin, and PSGL-1), Sigma Aldrich (alpha-1-acid glycoprotein and fetuin), and AbCam (EpCam). All other reagents were obtained from Sigma Aldrich unless otherwise noted.

Preparation of O-glycoproteomics samples. Five glycoprotein standards were combined to create a semi-complex mixture suitable for O-glycopeptide analysis: MUC16 (Q8WXI7.3), CD43 (P16150), GP1ba (P07359), Podocalyxin (O00592), and P-selectin glycoprotein ligand-1 (Q14242). For each protein, 30 micrograms were combined and dissolved in 50 mM Tris(tris(hydroxymethyl)aminomethane) (Tris), pH 8, before being digested with IMPa O-glycoprotease (Pseudomonas aeruginosa, NEB) with a 1:10 (w:w) glycoprotease:protein ratio. Digestion occurred over three hours at 37°C before the solution was brought to a final concentration of 10 mM tris(2-carboxyethyl)phosphine (TCEP) and 40 mM chloroacetamide (CAA). This was followed by an overnight (~14 h) digestion with trypsin (Promega) at 37°C with a 1:50 (w:w) protease:protein ratio. After digestion, peptides were desalted using Strata-X cartridges (Phenomenex) by conditioning the cartridge with 1 mL ACN followed by 1 mL 0.2% formic acid (FA) in water. Peptides were acidified with formic acid and then loaded onto the cartridge, followed by a 1 mL wash with 0.2% FA in water. Peptides were eluted with 400 µL of 0.2% FA in 80% ACN and dried via vacuum centrifugation.

Preparation of N-glycoproteomic samples. Seven glycoprotein standards were combined to create a semi-complex mixture suitable for N-glycopeptide analysis: alpha-1-acid glycoprotein (P02763), human fetuin (P02765), PD-L1 (Q9NZQ7), CD80/B7-1 (P33681), SARS-CoV-2 spike (P0DTC2), CD58/LFA-3 (P19256), and Epithelial cell adhesion molecule (P16422). Ten micrograms of each protein were dissolved in 50 mM Tris, combined and brought to a total concentration of 5% SDS using a 10% SDS stock solution, and digested using an S-trap mini (Protifi) following minor adaptations to the suppliers' protocol.[70] Briefly, cysteines were carbamidomethylated via incubation with 10 mM TCEP for 10 minutes at 60°C, followed by 40 mM CAA at room temperature for 60 minutes in the dark. Samples were acidified with phosphoric acid, and 7x volumes of bind/wash buffer (100 mM tetraethylammonium bromide (TEAB) in 90% methanol) were added. Samples were added to the trap and washed 3x with bind/wash buffer via centrifugation, followed by a 90-minute trypsin digestion at 47°C using a 1:25 protease:protein ratio. Following digestion, peptides were eluted with three washes: 1) 50 mM TEAB, 2) 0.2% formic acid in water, and 3) 0.2% formic acid in 50% ACN. The eluate was lyophilized and stored until LC-MS/MS analyses.

LC-MS/MS data acquisition. Samples were resuspended in 0.1% formic acid and approximately 1 µg of total peptide was injected per analysis. Each sample was analyzed by LC-MS/MS using the same Dionex UltiMate 3000 nano-LC system that was moved between an Orbitrap Ascend MultiOmics MS and an Orbitrap Eclipse MS that was housed in the same facility. All samples were measured with technical duplicate injections with a 90-minute total LC-MS/MS acquisition using a 25 cm Aurora Series Gen2 reverse-phase LC column (75 µm inner diameter packed with 1.6 µm FSC C18 particles, Ion Opticks). Peptides were loaded onto the column and eluted at a constant 300 nL/min flow rate using buffer A (0.1% formic acid in water) and B (0.1% formic acid in acetonitrile). The gradient was held at 1% B for 5 minutes, increased to 5% B from 5 to 5.1 minutes, increased from 5% B to 28% B from 5.1 to 70 minutes, increased to 95% B in 1 minute, held at 95% B for 5 minutes, and returned to 1% B to re-equilibrate the column for the remaining 14 minutes. LC conditions were identical for all analyses.

Standard O-glycopeptide analyses. Precursors were ionized at 1.8 kV, the inlet capillary temperature was held at 275°C, and the RF lens was set to 60%. Full MS scans were acquired with a resolution of 60k at 200 m/z, a normalized AGC target of 100% (400,000 charges), a maximum injection time of 123 ms (Ascend) or 118ms (Eclipse), and a scan range of 400-1800 m/z. Monoisotopic peptide filtering was enabled, dynamic exclusion was set at 60 seconds after 1 occurrence with a ±10 ppm window, a minimum intensity threshold of 50,000 was used, and charges 2-5 were selected for fragmentation. EThcD MS/MS scans were performed in a data-dependent fashion with a cycle time of 3 seconds, with constant parameters including a 2 m/z quadrupole isolation width for precursor ion isolation, an Orbitrap resolution of 60k at 200 m/z, a normalized AGC target set to 200% (100,000 charges), and a scan range of 120-4000 m/z. EThcD MS/MS scan parameters that were systematically evaluated in this study are summarized in **Table S1** and include a) a reagent anion target of 200,000 charges with 200 ms max injection time and static ion-ion reaction times of 30 ms, 50 ms, or 70 ms – or calibrated ion-ion reaction parameters;[71] b) maximum injection times of 100 ms or 150 ms; and c) supplemental HCD activation of 15%, 25%, and 35% normalized collision energy (NCE). These parameters were identical for Orbitrap Ascend and Orbitrap Eclipse data acquisition.

Fragmentation-specific O-glycopeptide analyses. To test the effects of specific fragmentation parameters, methods were created that performed multiple ETD and/or EThcD MS/MS scans on the same precursor ion. All LC and MS parameters described above remained the same unless noted, and all of these methods were only performed on the Orbitrap Ascend. For variable reaction time testing, precursor ions were selected in a data-dependent fashion for six subsequent MS/MS scans: ETD and EThcD using 30 ms ion-ion reaction time, ETD and EThcD using 50 ms ion-ion reaction time, and ETD and EThcD using calibrated ion-ion reaction time parameters. All EThcD scans used 25% NCE for supplemental activation, and the maximum injection times for all MS/MS scans was 150 ms. Individual methods were used that selected precursor charge states of either z = 2 or z = 3. For supplemental activation testing, precursor ions were selected in data-dependent fashion for four subsequent MS/MS scans: ETD, EThcD at 15% NCE, EThcD at 25% NCE, and EThcD at 35% NCE. All ion-ion reaction times were 50 ms with a reagent anion target of 200,000 charges, and only doubly protonated precursor ions were selected.

N-glycopeptide analyses. All LC and MS parameters outside of MS/MS settings remained identical for N-glycopeptide methods. All MS/MS scans used a scan range of 120-2000 m/z, a precursor isolation width of 2 m/z, and stepped collision energy HCD (sceHCD) with NCEs of 15%, 30%, and 45%. The resolution and maximum injection time were held constant at 60K and 150 ms while normalized AGC targets of 200%, 300%, 400%, and 500% were tested on both instruments (as discussed in the text), where 100% = 50,000 charges. Subsequent methods used a 300% AGC target setting when testing paired settings of varying Orbitrap resolutions and maximum injection times, with all resolutions defined at m/z 200 m/z. Methods on the Orbitrap Eclipse Orbitrap Eclipse had MS/MS scan resolutions of 15K, 30K, 50K, 60K, and 60K with maximum injection times of 43 ms, 54 ms, 86 ms, 118 ms, and 150 ms, respectively. Orbitrap Ascend had MS/MS scan resolutions of 22.5K, 30K, 45K, 60K, and 60K with maximum injection times of 43 ms, 59 ms, 91 ms, 123 ms, and 150 ms, respectively. All tested parameters are summarized in **Table S2**. Note, minor differences in injection times between the Eclipse and Ascend come from the dual IRM architecture that eliminates ~5 ms of overhead time on the Ascend to allow for more ion accumulation to occur per scan with no additional time cost to the duty cycle. In other words, the Eclipse and Ascend both collect FTMS2 with 60k resolving power spectra at 14.5 Hz; however, the Ascend has 59 ms of parallelizable injection time at this rate while the Eclipse only has 54 ms. Furthermore, because the Orbitrap central electrode on the Ascend operates at -4kV and the Orbitrap central electrode on the Eclipse operates at -5kV, resolution settings cannot be set the same between the two instruments. Instead, the most comparable settings were used (e.g., 45K on the Ascend vs. 50K on the Eclipse).

Data analysis. All searches were performed on a PC running Windows 10, with two 2.20 GHz Intel Xeon Silver 4114 CPU processors with 64 Gb of installed RAM, or on a PC running Windows 10, with two 3.00 GHz Intel Xeon W-2295 CPU processors with 128 Gb of installed RAM. Sixteen cores were used per search. O-glycopeptide raw data were searched using O-Pair Search implemented in MetaMorpheus (v.0.0320), which is available at https://github.com/smith-chem-wisc/MetaMorpheus.[72] The spectra were searched against a FASTA file containing Uniprot-derived sequences from all five proteins [Leukosialin (P16150), Mucin-16 (Q8WXI7.3), P-selectin Glycoprotein ligand 1 (Q14242), Podocalyxin (O00592), and Platelet glycoprotein Ib alpha chain (P07359)] as described by their sequences from the vendor, which was concatenated with decoy peptides by reversing sequences of the forward database. The “O-Glycopeptide Search” option was selected, where the O-glycopeptide search feature was enabled with an O-glycan database

of 22 common O-glycans (**Table S3**). The "Keep top N candidates" was set to 10, and the Data Type was set to EThcD or ETD. A mass tolerance of ±10 ppm was used for precursor ions and ±20 ppm for product ions. Methionine oxidation was specified as a variable modification with a maximum of 2 variable modifications per peptide, while carbamidomethylation of cysteine was set as a fixed modification. A combined IMPa and trypsin specificity was defined as previously described,[73] up to 12 missed cleavages were used (due to IMPa's cleavage behavior), and the maximum modification isoforms permitted was 1024. The oglyco.psmtsv results file was used, and the data was further filtered using C# scripts[59], some of which used the C# Mass Spectrometry Library (CSMSL, https://github.com/-dbaileychess/CSMSL). Only the highest quality (Level 1) identifications were used for further analysis. N-glycopeptide raw data were searched using the standalone Byonic environment (v. 3.11.3, Protein Metrics).[74,75] The spectra were searched against a FASTA file containing Uniprot-derived sequences from all seven proteins [Sars-CoV-2 spike (P0DTC2), PD-L1 (Q9NZQ7), CD80/B7-1 (P33681), Epithelial cell adhesion molecule (P16422), Lymphocyte function-associated antigen 3 (P19256), Alpha-1-acid glycoprotein (P02763), and Fetuin (P02765)], which was concatenated with a reversed sequence of the forward database. A 306 N-glycan database (**Table S4**) was used with glycan modifications denoted as common2 (meaning each glycan could occur twice per identified peptide). A mass tolerance of ± 10 and ± 20 ppm for the precursor and product ions was used, respectively, and fragmentation was set to HCD. Cleavage specificity was set as fully specific for C-terminal to R and K residues (fully tryptic) with two missed cleavages allowed, and protein FDR was set to 1%. The total common and rare max values were both set to 2. Carbamidomethylation (+57.021644) of cysteine was set as a fixed modification, and oxidation (+15.994915) of methionine was set as a rare2 variable modification. Following Byonic searching, results were filtered further as previously described,[59] with filtering metrics including a Byonic score greater than or equal to 200, a logProb value greater than or equal to 2, a deltaMod score greater than or equal to 10, and peptide length greater than 4 residues. To identify in-source fragmented N- and O-glycopeptides, we first generated a list of potential in-source fragmented glycopeptides, based on identical peptide backbones, identical elution profiles, and glycan composition subsets. These glycopeptides were quantified using the MS1 area under the curve in Skyline (version 24.1.1.284).[76]

RESULTS AND DISCUSSION

Architectural changes increase scan speed through the parallelization of ion populations

The architecture of the first generations of the quadrupole-Orbitrap-linear ion trap Tribrid MS platform enabled scan parallelization, especially when using the Orbitrap and linear ion trap (LIT) mass analyzers in combination.[40] A central feature of this architecture was the ion routing multipole (IRM) that served as the hub where all ions are initially accumulated and then transferred along for further manipulation (**Figure S1**). While this approach was a significant improvement over previous LIT-Orbitrap hybrid instruments, there were still major limitations when the ion trap was utilized for complex ion/ion manipulations (e.g., EThcD or MS^n scans) and the subsequent product ion population had to be moved back "upstream" past the IRM to the C-trap for Orbitrap m/z analysis. The newest generation Tribrid MS, the Orbitrap Ascend, houses several hardware changes, most notably the addition of a second IRM between the quadrupole and the C-trap (**Figure 1A**).[43,68] This "front" IRM enables precursor ion accumulation or HCD fragmentation in parallel with concurrent mass analysis in the Orbitrap and manipulation of a third population of ions using the "back" IRM and LIT. A practical effect of this architecture change is the ability to parallelize ion accumulation in the front IRM to minimize time losses from the overhead time needed for ion manipulations in the back IRM and LIT. This is especially apparent for EThcD scans that require the LIT for ion-ion reactions and the back IRM for supplemental activation. For

example, when holding ETD reaction time, reagent ion injection time, and Orbitrap transient time constant at 50 ms, 10 ms, and 128 ms (60k resolution at 200 m/z), respectively, the dual IRM architecture of the Orbitrap Ascend MultiOmics MS allows for an additional ~50 ms of "free" precursor ion accumulation time without a subsequent loss in scan acquisition speed relative to the single IRM format of the Orbitrap Eclipse (**Figure 1B**). Additionally, for any given precursor ion injection time between ~20-200 ms, the Ascend will provide faster spectral acquisition speeds. This can be especially advantageous in glycoproteomics, where sampling heterogenous glycopeptide populations demands fast acquisition speeds, longer ion accumulation times improve spectral quality of low abundance glycopeptides, and ETD-based methods can provide benefits for glycosite localization.[78–80]

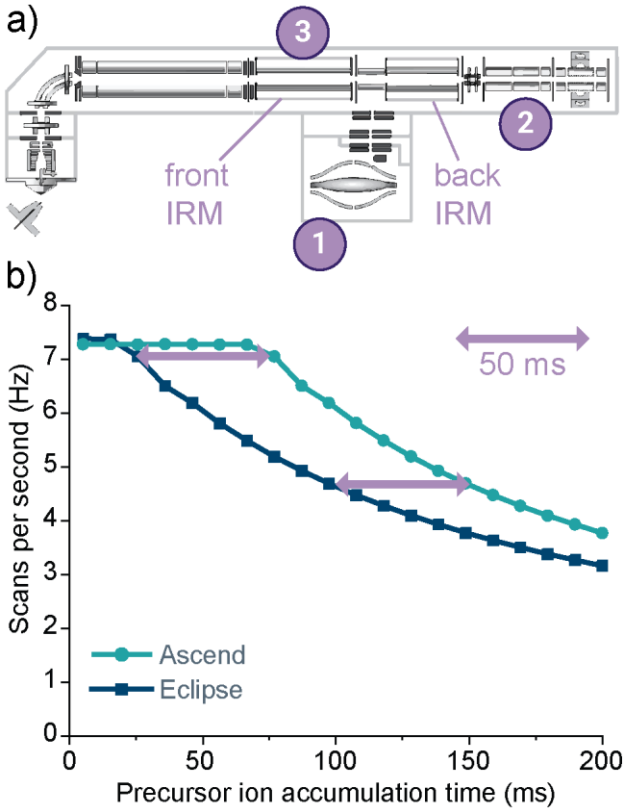

Figure 1. Architecture changes to the Orbitrap Tribrid MS platform provide more parallelization of scan functions. a) The addition of a second ion routing multipole (IRM) before the C-trap, i.e., the front IRM, on the Orbitrap Ascend MS allows simultaneous manipulation of three ion populations: 1) mass analysis in the Orbitrap, 2) tandem MS functions in the linear ion trap and back IRM, and 3) accumulation and/or beam-type collisional activation of precursor ions in the front IRM. **b)** When controlling for scan function overhead times like Orbitrap detection time (128 ms for a 60k resolution scan), a 50 ms ion-ion reaction time for ETD, and a 10 ms ETD reagent anion accumulation time, the dual IRM Tribrid architecture on the Orbitrap Ascend MS provides ~50 ms of additional precursor ion accumulation time without sacrificing scan acquisition speeds relative to the single IRM architecture on the Orbitrap Eclipse MS.

MS/MS scans and O-glycopeptide identifications

To systematically evaluate how the dual IRM instrument architecture can benefit glycoproteomics, we first focused on O-glycopeptide characterization using EThcD in a head-to-head

benchmarking experiment. There were several constants, including the mixture of O-glycopeptides used and all liquid chromatography variables. The same liquid chromatography system was wheeled between Orbitrap Eclipse and Orbitrap Ascend mass spectrometers housed in the same facility, and methods were identical between the two instruments, including gradient and scan parameters. The data-dependent EThcD methods themselves, all of which used a supplemental collision energy of 25% NCE, tested two variable types: ETD reaction time (30, 50, or 70 ms) and maximum precursor ion injection time (100 or 150 ms) (**Table S1**).

The top row in **Figure 2** shows data from both instruments for the 100 ms max injection time methods, while data from the 150 ms max injection time methods are in the bottom row. The Ascend acquired 20% to 29% more scans than the Eclipse for the tested ETD reaction times using a maximum injection time of 100 ms (**Figure 2a**) and 16% to 25% for scans using a maximum injection time of 150 ms (**Figure 2d**). This improvement across all methods highlights the improved scan acquisition speeds offered by the Ascend's dual IRM architecture. As expected, the largest increase in MS/MS scans was observed for the 70 ms ETD reaction times because the Eclipse must wait for the ETD reaction to complete and for ions to traverse the IRM and C-trap into the Orbitrap before accumulating a new packet of precursor ions. Additional EThcD MS/MS scans on the Ascend also translated to an increase in high-fidelity O-glycopeptide identifications relative to the Eclipse (**Figure 2b** and **2e**), although the increases in identification were not as substantial as the increase in MS/MS scans. This result is also somewhat expected, as the process of identifying O-glycopeptides is multifaceted and new, lower abundance precursor ions sampled in the additional MS/MS scans are simply more challenging to identify. All methods had an automatic gain control (AGC) setting for 100,000 charges, but both instruments only hit that target (i.e., hit the maximum injection time) for ~45-55% of scans for the 100 ms max injection time methods and ~20-25% of scans for the 150 ms maximum injection time methods. Thus, the Ascend likely would have shown even better performance across all conditions if a higher precursor ion target had been used. Regardless, the Ascend methods collected ~80 more EThcD MS/MS scans per minute than Eclipse methods for both methods as the majority of precursor ions were eluting from ~18-78 minutes (**Figure 2c** and **2f**).

Fine-tuning the ETD reaction time generates more O-glycopeptide identifications

One somewhat surprising result from the comparison of methods on the Ascend and Eclipse was the performance of the methods using a shorter ETD reaction time. More EThcD MS/MS scans with shorter ion-ion reaction times are expected (**Figure 2a** and **2d**), but we did not expect reaction times of 30 and 50 ms to consistently generate more identifications. This expectation is largely because O-glycopeptides tend to be predominantly doubly and triply-charged precursors, which typically use reaction times in the 40-100 ms range.[71,81] Thus, we expected shorter reaction times to generate underreacted precursor ions that would cause a decrease in identifications relative to the 70 ms reaction time. To investigate this further, we plotted the distribution of precursor ion charge states for O-glycopeptide identifications from the Ascend (**Figure 3a**). We also included data from methods that used calibrated ETD reaction parameters, where the optimal reaction time is determined for each charge state based on a calculated rate constant.[71] These calibrated ETD reaction parameters are intended to balance optimal product ion yield with acquisition speeds, but **Figure 3a** makes it clear that this setting is less effective than static ion-ion reaction times, at least in these experiments. **Figure 3b** shows the calibrated reaction times for each precursor ion charge state, highlighting that doubly charged precursors are being reacted for 2-3x longer than they are in the 30 and 50 ms static reaction time methods. There is a slight increase in the percentage of z =2 identifications as static reaction times increase closer to the calibrated reaction time of ~92 ms, which is to be expected based on the kinetics used for that calculation, but it is clear that reduced activation times under these acquisition conditions generate spectra that were amenable to O-glycopeptide identification. Indeed, the percentage of identified MS/MS scans and

the number of acquired scans increased as the ETD reaction time decreased, and both metrics were higher than at the calibrated reaction time (**Figure S2**).

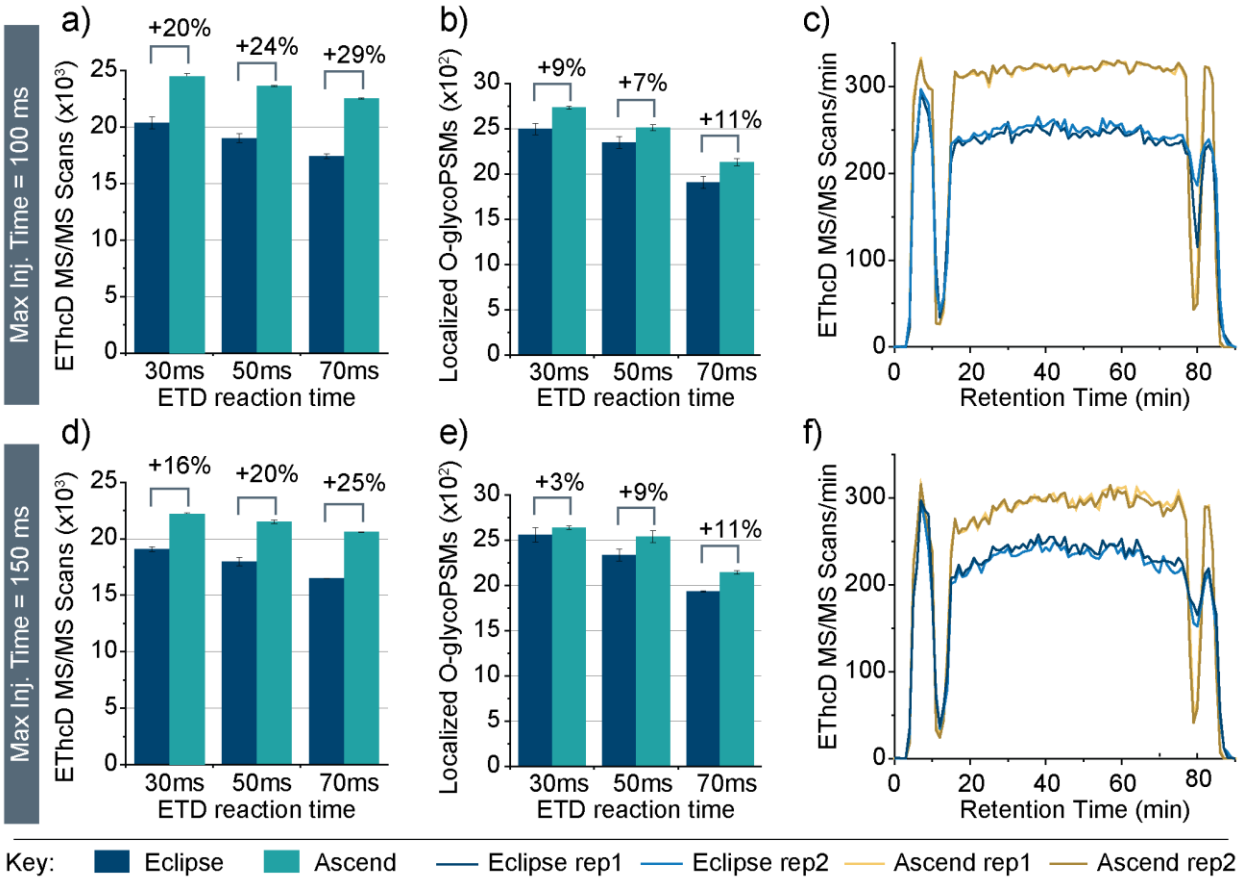

Figure 2. The dual IRM architecture of the Orbitrap Ascend MS generates more EThcD MS/MS scans and localized O-glycopeptides. An O-glycopeptide mixture was measured in technical duplicates on the Orbitrap Ascend MS and the Orbitrap Eclipse MS using EThcD fragmentation with 30, 50, and 70 ms ion-ion reaction times. Supplemental HCD activation was kept at 25% NCE. The top row shows data for methods using a 100 ms maximum precursor ion injection time (panels **a-c**), and the bottom row shows data for a 150 ms maximum injection time (panels **d-f**). The number of EThcD MS/MS scans (**a,d**) and O-glycopeptides (**b,e**) are compared for the Eclipse (navy) and Ascend (teal), with the percentage gain provided by the Ascend shown for each condition. All data here represent technical duplicate injections. Bar heights show replicate averages, and error bars show the individual replicates. When plotting scans per minute across 90-minute LC-MS/MS acquisitions using 50 ms reaction times (**c,f**), the Ascend was able to consistently acquire scans of about 80 more scans per minute during the time when the sample was eluting (starting at ~18 min).

We were intrigued by this result and sought to investigate fragment ion generation under these reaction conditions, especially as it relates to what reaction times can be used to optimize scan acquisition parameters with the dual IRM architecture of the Ascend. To do so, we designed a method where each precursor is selected in a data-dependent fashion for six subsequent MS/MS scans: ETD and EThcD at 25% NCE using a 30 ms static reaction time, a 50 ms static reaction time, or calibrated reaction parameters (**Figure 3c**). We ran this method twice, with each run only selecting for doubly or triply charged precursor ions. ETD is known to underperform for z = 2

precursor ions without supplemental activation, so we elected to focus on EThcD data that is widely used for O-glycopeptides. That said, we used ETD spectra to check for ETD-specific fragment ion types and degrees of unreacted precursors to help evaluate EThcD spectra (**Figure S3**). **Figure 3d** and **3e** plot the distribution of fragment ion intensity and fragment ion counts seen across the three reaction conditions for z = 2 and z = 3 precursor ions, respectively. ETD generates mainly c- and z•-type ions, with some y-type ion generation; supplemental HCD activation helps improve c- and z•-type ion generation by activating the non-dissociative electron transfer product while also generating b- and y-type ions from collisional dissociation of unreacted precursor ions.[82] Glycans are typically lost from b- and y-type ions when fragmenting O-glycopeptides with HCD; thus we only evaluated for non-modified b- and y-ion masses, but we extracted signal for c- and z•-type fragment ions that both retained or lost glycan masses. Surprisingly, the distribution of fragment types and their intensities from EThcD of z = 2 precursor ions remains relatively consistent for various ETD reaction times (**Figure 3d**). One exception was a slight increase in b- and y-ions for the MS/MS scans using an ETD reaction time of 30 ms, likely from the greater amount of unreacted precursor ions present with a shorter reaction time that generated more HCD-type fragments. For z = 3 precursor ions, the intensity and number of fragments for b-, y-, c-, z•-, and z•- glycan loss fragments from EThcD slightly increased for scans with 30 ms ion-ion reaction time (**Figure 3e**), but increases resulting from collisional activation of the unreacted precursor are less dominant. Triply protonated precursors resulted in more ETD-specific c- and z•-type ions due to a more effective ETD fragmentation reaction for precursors of higher charge states.[83,84] Interestingly, c-type ions did not show substantial glycan losses despite most c-type ions having a glycan modification (due to the nature of IMPa cleavage)[73,85]. Conversely, z•-type ions show more glycan loss, likely because they are less stable radical ions[86]. Altogether, these data show that shorter, static reaction times do not dramatically decrease fragment type count or intensity relative to calibrated reaction times. One explanation of these results could be a loss of the of the pseudo-first order kinetics that govern ion-ion reactions.[87] Here we used a 1:2 ratio of precursor: reagent ions for ETD reactions, which may have led to depletion of the excess reagent ion population needed to drive first order kinetics. This would mean the longer ETD reaction under the calibrated settings would not drive product ion generation at the same rate throughout the reaction time duration, which could reduce the benefit of using the calibrated settings. To explore this, we also examined fragment ion generation in ETD scans (instead of EThcD scans) collected in the same experiment (**Figure 3c**). The calibrated reaction time, along with the 30 ms and 50 ms reaction times, did not result in a clear difference in the number or intensity of b-, y-, c-, c-glycan loss, z•-, and z•- glycan loss fragments (**Figure S4**). This indicates that the reagent anion population may have been sufficiently depleted during the ETD reaction, causing a loss of pseudo-first order kinetics. The reagent ion target can be increased to regain pseudo-first order kinetics that may provide better performance for the calibrated reaction times; however, this would require longer reagent ion injection times, which would slow scan acquisition down further. Such an increase in time per scan would likely result in fewer MS/MS scans that could offset benefits gained from increased product ion generation. Overall, using shorter 30-50 ms static reaction times for all precursor ion charge states can increase scan speed to generate more O-glycopeptide identifications without significant sacrifices to spectral quality.

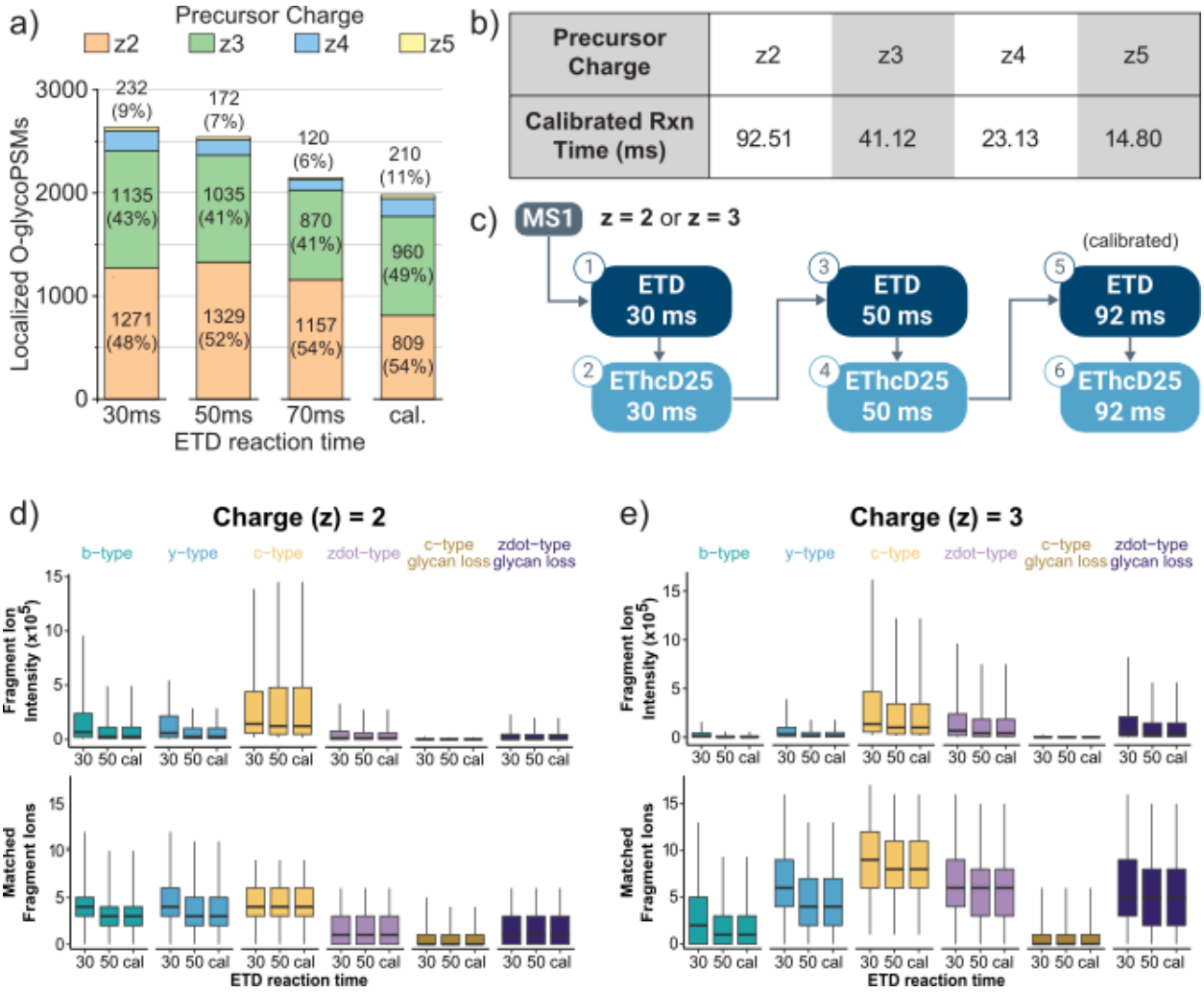

Figure 3. Comparing static and calibrated ion-ion reaction times for O-glycopeptide EThcD spectra. **a)** Localized O-glycopeptide spectral matches, broken down by precursor ion charge state, from Ascend data using 30 ms, 50 ms, 70 ms, or calibrated ion-ion reaction times. Numbers and percentages from each charge state are provided, with z = 4 and z = 5 presented in aggregate. **b)** A table showing calibrated reaction times that were automatically determined on the Ascend. **c)** Method design to investigate the influence of ion-ion reaction time on fragment ion production. Each precursor is selected for six subsequent MS/MS scans. In panels **d** and **e**, distributions of fragment ion intensity (top) and count (bottom) are shown for localized O-glycopeptides identified from EThcD spectra with varying ion-ion reaction times for z = 2 and z = 3 precursor ions, respectively. Fragment ion types are separated out by type, including b-, y-, c-, z•-, c-glycan loss fragments, and z•-glycan loss fragments. Boxes represent first and third quartiles, and the median is shown with a black bar. Whiskers show 10-90 percentiles.

Optimizing supplemental collisional energy in EThcD scans is important

Supplemental activation, often through collisional or photoactivation, is particularly useful for ETD,[78–80,82,88] especially for low-charge density precursors that are typically generated by O-glycoproteomics samples.[89] Non-covalent interactions can hold c- and z•-type fragment ions together in the gas phase, a process called electron transfer without dissociation (ETnoD). In EThcD, the supplemental HCD activates the ETnoD product to increase c- and z•-type fragment ion generation, and it also fragments unreacted precursor to generate b- and y-type fragment ions typical of collisional dissociation.[67,82] Often the collisional activation of EThcD is enough to provide

supplemental energy to improve c- and z•-type fragment ion yield while not over-fragmenting to cause losses of these useful ETD-specific fragments. The b- and y-ion generation from supplemental HCD can also prove helpful for identifying glycopeptides (and other species). This balance is important for O-glycopeptides, where O-glycans are particularly labile. Based on our surprising results above that shorter static reaction times could provide a similar fragment ion signal as calibrated reaction times, especially for z = 2 precursor ions, we also investigated the effect of supplemental HCD activation energies (15%, 25%, and 35% NCE) for EThcD at different ion-ion reaction times on the Ascend. **Figure 4a** shows that increasing EThcD supplemental activation energy led to a dramatic increase in O-glycopeptide identifications.

We set up a method specifically designed to compare fragmentation between ETD and EThcD at 15%, 25%, and 35% NCE. All reaction times were held constant at 50 ms, and only doubly charged precursor ions were selected for tandem MS. Each precursor ion was selected for four MS/MS scans, as shown in **Figure 4b**. We extracted b-, y-, c-, z•-, c-glycan loss, and z•-glycan loss-ions from scans from all localized O-glycopeptide spectral matches, and **Figure 4c** shows their distribution for each condition. As supplemental HCD collision energy increases, there was a consistent increase in all fragment ion types investigated. Despite small and noticeable increases in c-glycan-loss and z•-glycan loss-ions with increasing supplemental activation energy, there was not a substantial decrease in c- and z•-type ions that are crucial for O-glycosite localization. This increase across all ion types partially explains increases in O-glycopeptide identifications, but what is particularly relevant are increases in four of these fragments (b-, y-, c-glycan loss, and z•-glycan loss) that are "unmodified" (gray boxes in **Figure 4c**). In other words, they can be used by search engines to identify peptides without needing to know the glycan modifications. This information is especially critical in the fragment ion indexing[72,90] approach used in high-performing O-glycopeptide search algorithms like O-Pair Search (used here) that cannot account for modification status prior to indexing. Thus, besides increasing all fragment ion yields, EThcD at higher collision energies uniquely benefits from the generation of non-glycan-retaining fragments that aid in peptide identification. Simultaneously, EThcD under these conditions did not generate substantial losses of localization-critical c and z•-type ions that retain O-glycans. This shows that higher EThcD collision energies may be broadly beneficial for O-glycoproteomics, although instrument differences should be evaluated for each experiment.

Comparing N-glycopeptide identifications on the Eclipse and Ascend

Beyond the benefits for EThcD-based O-glycopeptide characterization, we also investigated the performance of the Orbitrap Ascend for sceHCD-based methods for N-glycopeptides relative to the Orbitrap Eclipse. The dual IRM architecture on the Ascend eliminates ~5 ms of overhead time to allow for more ion accumulation to occur per OT acquisition with no additional time cost to acquisition rate, which can benefit N-glycopeptide identifications.[68] To understand how the Ascend could benefit various N-glycoproteomics methods, we set up a similar head-to-head comparison between the Ascend and Eclipse with identical N-glycopeptide sample, gradient, and most scan parameters. Subtle differences, e.g., Orbitrap resolution for MS/MS scans and parallelizable injection times for a given Orbitrap transient, meant that some methods varied slightly between the two instruments, but methods using various Orbitrap resolutions and corresponding maximum injection time were compared for the Eclipse and Ascend (**Figure 5a**). Here, we did test for optimal precursor ion AGC target and used 150,000 ions as the target for all subsequent methods (**Figure S5**).

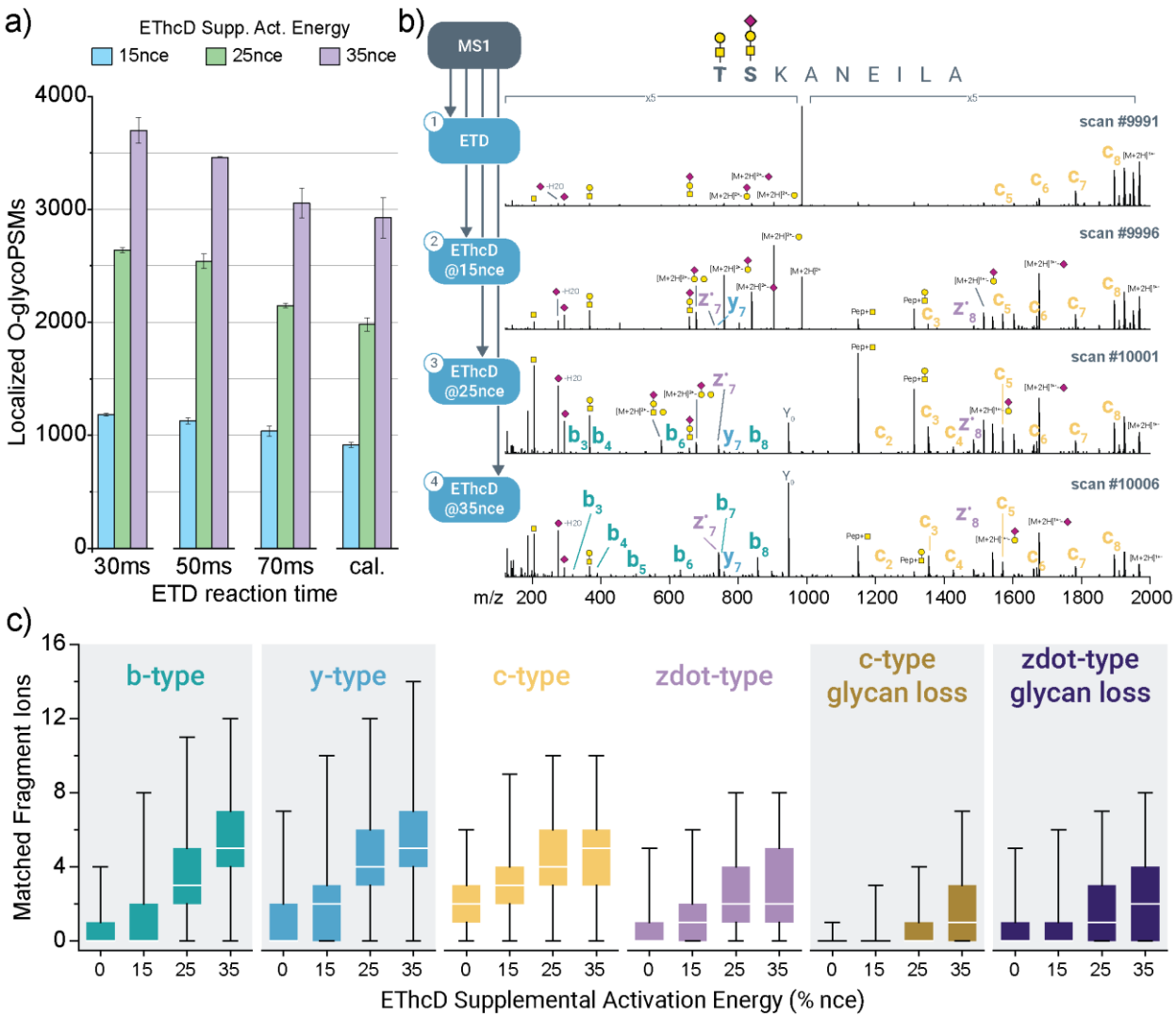

Figure 4. Effects of EThcD supplemental activation energy on O-glycopeptide identifications and fragment ion generation. a) O-glycopeptide spectral matches using various ion-ion reaction times and EThcD supplemental activation energies of 15%, 25%, or 35% NCE. **b)** Method design used to collect O-glycopeptide spectra at different collision energies on the Orbitrap Ascend. An example doubly glycosylated O-glycopeptide shows annotated spectra collected using this data-dependent acquisition scheme that acquired four MS/MS spectra per precursor ion. **c)** The distribution of fragment ion counts, delineated by fragment ion types, for localized O-glycopeptide identifications each of the EThcD supplemental collision energies used. All scans used a 50 ms ETD reaction time. Boxes in box plots represent first and third quartiles, and the median is shown with a black bar. Whiskers show 10-90 percentiles. The gray boxes denote “unmodified” fragment ion types, i.e., those that do not retain glycan modifications.

The Ascend consistently generated more sceHCD MS/MS scans during the 15-84 min window in the gradient when the sample eluted (**Figure 5b**), although the differences were less dramatic than with the EThcD-based methods above. This is expected because the scan overhead time of sceHCD is already low, meaning these types of scans do not slow down the Eclipse as much as EThcD. Despite only modest gains in MS/MS scans acquired, the faster sceHCD methods generated noticeably more N-glycopeptide identifications on the Ascend (**Figure 5c**), especially for methods with faster scan rates. This benefit can be explained by the improvements in ion accumulation allowed by the front IRM on the Ascend, as well as by other hardware improvements

that increase ion transmission (**Figure S5**).[68] When looking at scan acquisition rates on the Ascend and Eclipse for each method, it is clear that the Eclipse has maximized its spectral acquisition rate in all experiments, as evidenced by the mostly flat lines in **Figure 5d**. On the Ascend, however, these methods did not consistently run at the maximum acquisition speed, as seen by the fluctuating lines. This means that the lower-resolution, high-scan-acquisition-rate Ascend methods could likely be further optimized to make use of all parallelizable time. Or, alternatively, the LC-MS method could be shortened to increase sample throughput. For slower sceHCD methods, the difference in scan acquisition rate between the Ascend and the Eclipse is marginal when using "all parallelizable injection time", e.g., 60k resolution with 118 ms (Eclipse) or 123 ms (Ascend) maximum injection time. However, for the method that increased the maximum injection time to 150 ms, meaning the instrument potentially sits idle for tens of milliseconds, it is clear that this "idle time" is less detrimental to the scan acquisition rate using the front IRM accumulation of the Ascend. Overall, these data show that the dual IRM architecture can benefit N-glycoproteomics with sceHCD methods, especially when balancing scan rates with necessary ion accumulation times. As a final note, we examined N- and O-glycopeptides for evidence of in-source fragmentation on the two instruments and found a small number of in-source fragmented glycopeptides that could be reliably assigned based on identical peptide backbones, identical elution profiles, and glycan composition subsets (**File S1** and **S2**). We did not observe a notable difference between in-source fragmentation rates between the Ascend and the Eclipse (**Figure S6**).

CONCLUSIONS

Advances in instrumentation are crucial for improving glycoproteomics throughput and data quality. Orbitrap Tribrid mass spectrometers have proven beneficial for N- and O-glycoproteomics, due to their flexibility and sensitivity. The newest generation Orbitrap Tribrid, the Orbitrap Ascend, introduced a dual ion routing multipole architecture that substantially improves parallel manipulation of ion populations. Here, we report how this dual IRM infrastructure on the Ascend can benefit on O- and N-glycopeptide identifications. For EThcD-based O-glycopeptide analyses, we demonstrated how the front IRM significantly improves scan acquisition rate, which in turn improves localized O-glycopeptide identifications. We also saw interesting trends in ion-ion reaction times and supplemental HCD activation energies used for EThcD, suggesting that shorter, static reaction times (e.g., 30 or 50 ms) and relatively high (35% NCE) supplemental activation energies may be most beneficial for improve O-glycopeptide identifications, especially when considering the benefits in scan acquisition rates provided by the Ascend. We also show how balancing scan rate and ion injection time for N-glycopeptide characterization can benefit from hardware improvements on the Ascend. In all, this study underscores the utility of the Orbitrap Ascend for glycoproteomic analyses and highlights the value in careful evaluation of dissociation methods to maximize the number of informative spectra for glycopeptide identification.

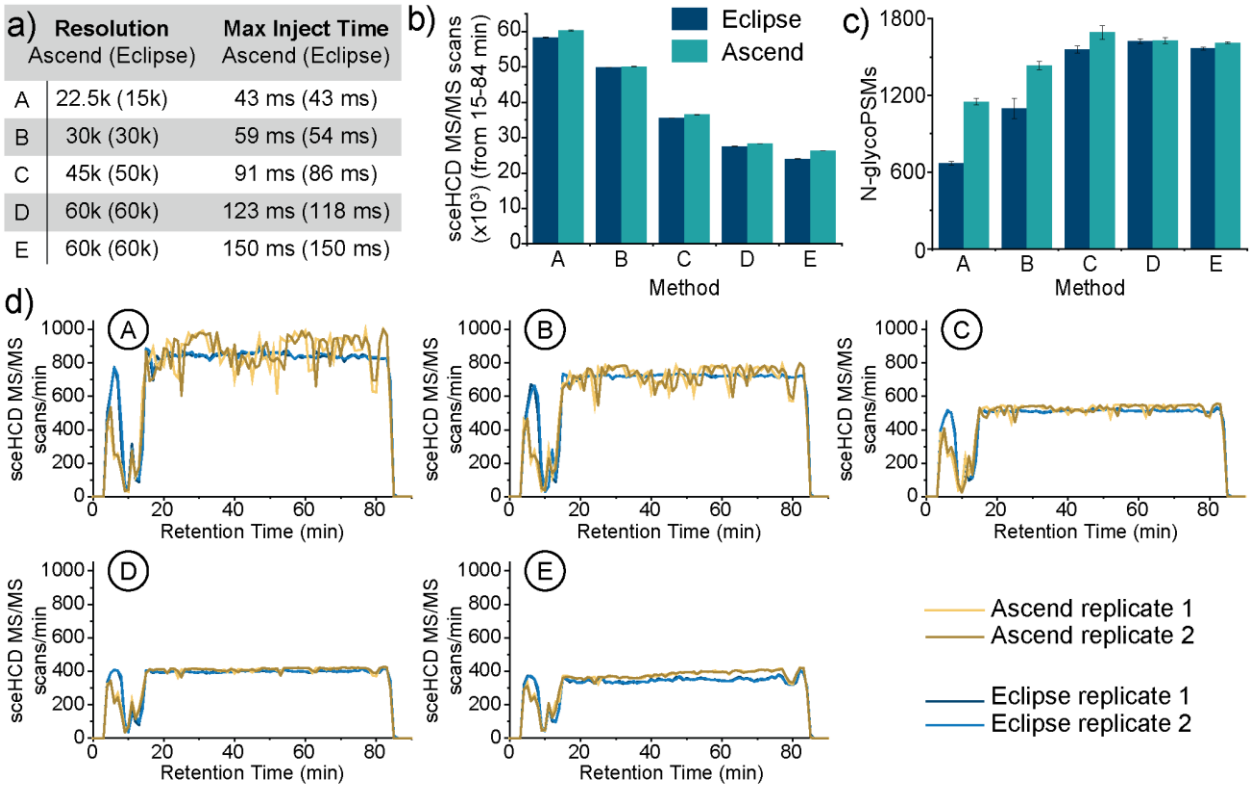

Figure 5. N-glycopeptide identifications with sceHCD methods on the Orbitrap Ascend and Orbitrap Eclipse. a) Five different sceHCD methods were tested for N-glycopeptide identification, where Orbitrap resolution and corresponding maximum parallizeable injection time (and by extension, scan acquisition speeds) were varied. The number of sceHCD MS/MS scans (**b**) and N-glycopeptides (**c**) are compared for the Eclipse (navy) and Ascend (teal). All data here represent technical duplicate injections. Bar heights show replicate averages and error bars show the individual replicates. **d)** Comparisons of sceHCD MS/MS scans per minute for the Ascend and the Eclipse across 90-minute LC-MS/MS acquisitions using various resolution and maximum precursor injection time settings.

NOTES, COMPETING FINANCIAL INTERESTS, AND AUTHOR CONTRIBUTIONS

J.H., D.B., A.E.L., R.D.M., W.D.B., J.C., V.Z., G.C.M., and C.M. are employees of Thermo Fisher Scientific, the manufacturer of the instrumentation used in this research. N.M.R. receives support from Thermo Fisher Scientific under a nondisclosure agreement and is a consultant for Tegmine Therapeutics, Cartography Biosciences, and Augment Biologics. Experiments described in this manuscript were conducted on instruments housed in a Thermo Fisher Scientific facility. Conceptualization, N.M.R., G.C.M., and C.M..; methodology, N.M.R., J.H., D.B., A.E.L., R.D.M., W.D.B., J.C., V.Z., G.C.M., and C.M.; investigation, N.M.R., T.S.V. E.S., R.Z., K.A.M., and A.G.D.; writing – original draft, T.S.V. E.S., R.Z., K.A.M., A.G.D., and N.M.R.; writing – review & editing, T.S.V., E.S., and N.M.R. with input from all authors.

SUPPORTING INFORMATION

Supporting Information, including Figures S1-4, Tables S1-4, and Files S1-2, is available free of charge online.

ACKNOWLEDGEMENTS

Research reported in this publication was supported by the National Institutes of Health under Award Numbers R00GM147304 and P41GM108538 (N.M.R), by an ASMS Research Award, and by a Washington Research Foundation Postdoctoral Fellowship (E.S). We thank Lei Lu and Michael Shortreed for helpful discussions about MetaMorpheus and John E.P. Syka for helpful discussions throughout this study.

REFERENCES

(1) *Essentials of Glycobiology*, 4th ed.; Varki, A., Cummings, R. D., Esko, J. D., Stanley, P., Hart, G. W., Aebi, M., Mohnen, D., Kinoshita, T., Packer, N. H., Prestegard, J. H., Schnaar, R. L., Seeberger, P. H., Eds.; Cold Spring Harbor Laboratory Press: Cold Spring Harbor (NY), 2022.

(2) Apweiler, R.; Hermjakob, H.; Sharon, N. On the Frequency of Protein Glycosylation, as Deduced from Analysis of the SWISS-PROT Database1. *Biochim. Biophys. Acta BBA - Gen. Subj.* **1999**, *1473* (1), 4–8. https://doi.org/10.1016/S0304-4165(99)00165-8.

(3) Smith, B. A. H.; Bertozzi, C. R. The Clinical Impact of Glycobiology: Targeting Selectins, Siglecs and Mammalian Glycans. *Nat. Rev. Drug Discov.* **2021**, *20* (3), 217–243. https://doi.org/10.1038/s41573-020-00093-1.

(4) Reily, C.; Stewart, T. J.; Renfrow, M. B.; Novak, J. Glycosylation in Health and Disease. *Nat. Rev. Nephrol.* **2019**, *15* (6), 346–366. https://doi.org/10.1038/s41581-019-0129-4.

(5) Rodríguez, E.; Schetters, S. T. T.; Van Kooyk, Y. The Tumour Glyco-Code as a Novel Immune Checkpoint for Immunotherapy. *Nat. Rev. Immunol.* **2018**, *18* (3), 204–211. https://doi.org/10.1038/nri.2018.3.

(6) Schjoldager, K. T.; Narimatsu, Y.; Joshi, H. J.; Clausen, H. Global View of Human Protein Glycosylation Pathways and Functions. *Nat. Rev. Mol. Cell Biol. 2020 2112* **2020**, *21* (12), 729–749. https://doi.org/10.1038/s41580-020-00294-x.

(7) Sun, S.; Hu, Y.; Ao, M.; Shah, P.; Chen, J.; Yang, W.; Jia, X.; Tian, Y.; Thomas, S.; Zhang, H. N-GlycositeAtlas: A Database Resource for Mass Spectrometry-Based Human N-Linked Glycoprotein and Glycosylation Site Mapping. *Clin. Proteomics* **2019**, *16* (1), 1–11. https://doi.org/10.1186/s12014-019-9254-0.

(8) Wulff-Fuentes, E.; Berendt, R. R.; Massman, L.; Danner, L.; Malard, F.; Vora, J.; Kahsay, R.; Olivier-Van Stichelen, S. The Human O-GlcNAcome Database and Meta-Analysis. *Sci. Data* **2021**, *8* (1), 25. https://doi.org/10.1038/s41597-021-00810-4.

(9) Steentoft, C.; Vakhrushev, S. Y.; Joshi, H. J.; Kong, Y.; Vester-Christensen, M. B.; Schjoldager, K. T.-B. G.; Lavrsen, K.; Dabelsteen, S.; Pedersen, N. B.; Marcos-Silva, L.; Gupta, R.; Paul Bennett, E.; Mandel, U.; Brunak, S.; Wandall, H. H.; Levery, S. B.; Clausen, H. Precision Mapping of the Human O-GalNAc Glycoproteome through SimpleCell Technology. *EMBO J.* **2013**, *32* (10), 1478–1488. https://doi.org/10.1038/emboj.2013.79.

(10) Stanley, P.; Moremen, K. W.; Lewis, N. E.; Taniguchi, N.; Aebi, M. N-Glycans. In *Essentials of Glycobiology*; Varki, A., Cummings, R. D., Esko, J. D., Stanley, P., Hart, G. W., Aebi, M., Mohnen, D., Kinoshita, T., Packer, N. H., Prestegard, J. H., Schnaar, R. L., Seeberger, P. H., Eds.; Cold Spring Harbor Laboratory Press: Cold Spring Harbor (NY), 2022.

(11) Esmail, S.; Manolson, M. F. Advances in Understanding *N*-Glycosylation Structure, Function, and Regulation in Health and Disease. *Eur. J. Cell Biol.* **2021**, *100* (7), 151186. https://doi.org/10.1016/j.ejcb.2021.151186.

(12) Lin, Y.; Lubman, D. M. The Role of *N*-Glycosylation in Cancer. *Acta Pharm. Sin. B* **2024**, *14* (3), 1098–1110. https://doi.org/10.1016/j.apsb.2023.10.014.

(13) Wandall, H. H.; Nielsen, M. A. I.; King-Smith, S.; de Haan, N.; Bagdonaite, I. Global Functions of O-Glycosylation: Promises and Challenges in O-Glycobiology. *FEBS J.* **2021**. https://doi.org/10.1111/FEBS.16148.
(14) Magalhães, A.; Duarte, H. O.; Reis, C. A. The Role of O-Glycosylation in Human Disease. *Mol. Aspects Med.* **2021**, *79*, 100964. https://doi.org/10.1016/j.mam.2021.100964.
(15) Riley, N. M.; Wen, R. M.; Bertozzi, C. R.; Brooks, J. D.; Pitteri, S. J. Measuring the Multifaceted Roles of Mucin-Domain Glycoproteins in Cancer. In *Advances in Cancer Research*; Academic Press, 2022. https://doi.org/10.1016/bs.acr.2022.09.001.
(16) Wisnovsky, S.; Bertozzi, C. R. Reading the Glyco-Code: New Approaches to Studying Protein–Carbohydrate Interactions. *Curr. Opin. Struct. Biol.* **2022**, *75*, 102395. https://doi.org/10.1016/j.sbi.2022.102395.
(17) Ruhaak, L. R.; Xu, G.; Li, Q.; Goonatilleke, E.; Lebrilla, C. B. Mass Spectrometry Approaches to Glycomic and Glycoproteomic Analyses. *Chem. Rev.* **2018**, *118* (17), 7886–7930. https://doi.org/10.1021/acs.chemrev.7b00732.
(18) Bagdonaite, I.; Malaker, S. A.; Polasky, D. A.; Riley, N. M.; Schjoldager, K.; Vakhrushev, S. Y.; Halim, A.; Aoki-Kinoshita, K. F.; Nesvizhskii, A. I.; Bertozzi, C. R.; Wandall, H. H.; Parker, B. L.; Thaysen-Andersen, M.; Scott, N. E. Glycoproteomics. *Nat. Rev. Methods Primer* **2022**, *2* (1), 1–29. https://doi.org/10.1038/s43586-022-00128-4.
(19) Oliveira, T.; Thaysen-Andersen, M.; Packer, N. H.; Kolarich, D. The Hitchhiker's Guide to Glycoproteomics. *Biochem. Soc. Trans.* **2021**, *49* (4), 1643–1662. https://doi.org/10.1042/BST20200879.
(20) Riley, N. M.; Bertozzi, C. R.; Pitteri, S. J. A Pragmatic Guide to Enrichment Strategies for Mass Spectrometry–Based Glycoproteomics. *Mol. Cell. Proteomics* **2021**, *20*, 100029. https://doi.org/10.1074/MCP.R120.002277.
(21) Li, Y.; Qin, H.; Ye, M. An Overview on Enrichment Methods for Cell Surface Proteome Profiling. *J. Sep. Sci.* **2020**, *43* (1), 292–312. https://doi.org/10.1002/jssc.201900700.
(22) Chang, D.; Zaia, J. Methods to Improve Quantitative Glycoprotein Coverage from Bottom-up LC-MS Data. *Mass Spectrom. Rev.* **2022**, *41* (6), 922–937. https://doi.org/10.1002/mas.21692.
(23) Suttapitugsakul, S.; Sun, F.; Wu, R. Recent Advances in Glycoproteomic Analysis by Mass Spectrometry. *Anal. Chem.* **2020**, *92* (1), 267–291. https://doi.org/10.1021/acs.analchem.9b04651.
(24) Polasky, D. A.; Nesvizhskii, A. I. Recent Advances in Computational Algorithms and Software for Large-Scale Glycoproteomics. *Curr. Opin. Chem. Biol.* **2023**, *72*, 102238. https://doi.org/10.1016/j.cbpa.2022.102238.
(25) Abrahams, J. L.; Taherzadeh, G.; Jarvas, G.; Guttman, A.; Zhou, Y.; Campbell, M. P. Recent Advances in Glycoinformatic Platforms for Glycomics and Glycoproteomics. *Curr. Opin. Struct. Biol.* **2020**, *62*, 56–69. https://doi.org/10.1016/j.sbi.2019.11.009.
(26) Thomas, D. R.; Scott, N. E. Glycoproteomics: Growing up Fast. *Curr. Opin. Struct. Biol.* **2021**, *68*, 18–25. https://doi.org/10.1016/j.sbi.2020.10.028.
(27) Chernykh, A.; Kawahara, R.; Thaysen-Andersen, M. Towards Structure-Focused Glycoproteomics. *Biochem. Soc. Trans.* **2021**, *49* (1), 161–186. https://doi.org/10.1042/BST20200222.
(28) Hu, H.; Khatri, K.; Klein, J.; Leymarie, N.; Zaia, J. A Review of Methods for Interpretation of Glycopeptide Tandem Mass Spectral Data. *Glycoconj. J.* **2016**, *33* (3), 285–296. https://doi.org/10.1007/s10719-015-9633-3.
(29) Cao, W. Advancing Mass Spectrometry–Based Glycoproteomic Software Tools for Comprehensive Site-Specific Glycoproteome Analysis. *Curr. Opin. Chem. Biol.* **2024**, *80*, 102442. https://doi.org/10.1016/j.cbpa.2024.102442.

(30) Peters-Clarke, T. M.; Coon, J. J.; Riley, N. M. Instrumentation at the Leading Edge of Proteomics. *Anal. Chem.* **2024**, *96* (20), 7976–8010. https://doi.org/10.1021/acs.analchem.3c04497.
(31) Plank, M. J. Modern Data Acquisition Approaches in Proteomics Based on Dynamic Instrument Control. *J. Proteome Res.* **2022**, *21* (5), 1209–1217. https://doi.org/10.1021/acs.jproteome.2c00096.
(32) Trujillo, E. A.; Hebert, A. S.; Brademan, D. R.; Coon, J. J. Maximizing Tandem Mass Spectrometry Acquisition Rates for Shotgun Proteomics. *Anal. Chem.* **2019**, *91* (20), 12625–12629. https://doi.org/10.1021/acs.analchem.9b02979.
(33) Fröhlich, K.; Fahrner, M.; Brombacher, E.; Seredynska, A.; Maldacker, M.; Kreutz, C.; Schmidt, A.; Schilling, O. Data-Independent Acquisition: A Milestone and Prospect in Clinical Mass Spectrometry-Based Proteomics. *Mol. Cell. Proteomics* **2024**, 100800. https://doi.org/10.1016/j.mcpro.2024.100800.
(34) Messner, C. B.; Demichev, V.; Wang, Z.; Hartl, J.; Kustatscher, G.; Mülleder, M.; Ralser, M. Mass Spectrometry-Based High-Throughput Proteomics and Its Role in Biomedical Studies and Systems Biology. *PROTEOMICS* **2023**, *23* (7–8), 2200013. https://doi.org/10.1002/pmic.202200013.
(35) Beckman, J. S.; Voinov, V. G.; Hare, M.; Sturgeon, D.; Vasil'ev, Y.; Oppenheimer, D.; Shaw, J. B.; Wu, S.; Glaskin, R.; Klein, C.; Schwarzer, C.; Stafford, G. Improved Protein and PTM Characterization with a Practical Electron-Based Fragmentation on Q-TOF Instruments. *J. Am. Soc. Mass Spectrom.* **2021**, *32* (8), 2081–2091. https://doi.org/10.1021/JASMS.0C00482.
(36) Baba, T.; Ryumin, P.; Duchoslav, E.; Chen, K.; Chelur, A.; Loyd, B.; Chernushevich, I. Dissociation of Biomolecules by an Intense Low-Energy Electron Beam in a High Sensitivity Time-of-Flight Mass Spectrometer. *J. Am. Soc. Mass Spectrom.* **2021**, *32* (8), 1964–1975. https://doi.org/10.1021/JASMS.0C00425.
(37) Armony, G.; Brehmer, S.; Srikumar, T.; Pfennig, L.; Zijlstra, F.; Trede, D.; Kruppa, G.; Lefeber, D. J.; van Gool, A. J.; Wessels, H. J. C. T. The GlycoPaSER Prototype as a Real-Time N-Glycopeptide Identification Tool Based on the PaSER Parallel Computing Platform. *Int. J. Mol. Sci.* **2023**, *24* (9), 7869. https://doi.org/10.3390/ijms24097869.
(38) Feng, X.; Shu, H.; Zhang, S.; Peng, Y.; Zhang, L.; Cao, X.; Wei, L.; Lu, H. Relative Quantification of N-Glycopeptide Sialic Acid Linkage Isomers by Ion Mobility Mass Spectrometry. *Anal. Chem.* **2021**, *93* (47), 15617–15625. https://doi.org/10.1021/acs.analchem.1c02803.
(39) Macauslane, K. L.; Pegg, C. L.; Nouwens, A. S.; Kerr, E. D.; Seitanidou, J.; Schulz, B. L. Electron-Activated Dissociation and Collision-Induced Dissociation Glycopeptide Fragmentation for Improved Glycoproteomics. *Anal. Chem.* **2024**, *96* (27), 10986–10994. https://doi.org/10.1021/acs.analchem.4c01450.
(40) Senko, M. W.; Remes, P. M.; Canterbury, J. D.; Mathur, R.; Song, Q.; Eliuk, S. M.; Mullen, C.; Earley, L.; Hardman, M.; Blethrow, J. D.; Bui, H.; Specht, A.; Lange, O.; Denisov, E.; Makarov, A.; Horning, S.; Zabrouskov, V. Novel Parallelized Quadrupole/Linear Ion Trap/Orbitrap Tribrid Mass Spectrometer Improving Proteome Coverage and Peptide Identification Rates. *Anal. Chem.* **2013**, *85* (24), 11710–11714. https://doi.org/10.1021/ac403115c.
(41) Levy, M. J.; Washburn, M. P.; Florens, L. Probing the Sensitivity of the Orbitrap Lumos Mass Spectrometer Using a Standard Reference Protein in a Complex Background. *J. Proteome Res.* **2018**, *17* (10), 3586–3592. https://doi.org/10.1021/acs.jproteome.8b00269.
(42) Yu, Q.; Paulo, J. A.; Naverrete-Perea, J.; McAlister, G. C.; Canterbury, J. D.; Bailey, D. J.; Robitaille, A. M.; Huguet, R.; Zabrouskov, V.; Gygi, S. P.; Schweppe, D. K. Benchmarking the Orbitrap Tribrid Eclipse for Next Generation Multiplexed Proteomics. *Anal. Chem.* **2020**, *92* (9), 6478–6485. https://doi.org/10.1021/acs.analchem.9b05685.

(43) Shuken, S. R.; McAlister, G. C.; Barshop, W. D.; Canterbury, J. D.; Bergen, D.; Huang, J.; Huguet, R.; Paulo, J. A.; Zabrouskov, V.; Gygi, S. P.; Yu, Q. Deep Proteomic Compound Profiling with the Orbitrap Ascend Tribrid Mass Spectrometer Using Tandem Mass Tags and Real-Time Search. *Anal. Chem.* **2023**, *95* (41), 15180–15188. https://doi.org/10.1021/acs.analchem.3c01701.
(44) Chau, T. H.; Chernykh, A.; Kawahara, R.; Thaysen-Andersen, M. Critical Considerations in *N*-Glycoproteomics. *Curr. Opin. Chem. Biol.* **2023**, *73*, 102272. https://doi.org/10.1016/j.cbpa.2023.102272.
(45) Pap, A.; Kiraly, I. E.; Medzihradszky, K. F.; Darula, Z. Multiple Layers of Complexity in O-Glycosylation Illustrated With the Urinary Glycoproteome. *Mol. Cell. Proteomics* **2022**, *21* (12). https://doi.org/10.1016/j.mcpro.2022.100439.
(46) Darula, Z.; Medzihradszky, K. F. Analysis of Mammalian O-Glycopeptides - We Have Made a Good Start, but There Is a Long Way to Go. *Mol. Cell. Proteomics* **2018**, *17* (1), 2–17. https://doi.org/10.1074/mcp.MR117.000126.
(47) Riley, N. M.; Mullen, C.; Weisbrod, C. R.; Sharma, S.; Senko, M. W.; Zabrouskov, V.; Westphall, M. S.; Syka, J. E. P.; Coon, J. J. Enhanced Dissociation of Intact Proteins with High Capacity Electron Transfer Dissociation. *J. Am. Soc. Mass Spectrom.* **2016**, *27* (3), 520–531. https://doi.org/10.1007/s13361-015-1306-8.
(48) Espadas, G.; Borràs, E.; Chiva, C.; Sabidó, E. Evaluation of Different Peptide Fragmentation Types and Mass Analyzers in Data-Dependent Methods Using an Orbitrap Fusion Lumos Tribrid Mass Spectrometer. *PROTEOMICS* **2017**, *17* (9), 1600416. https://doi.org/10.1002/pmic.201600416.
(49) Fornelli, L.; Srzentić, K.; Toby, T. K.; Doubleday, P. F.; Huguet, R.; Mullen, C.; Melani, R. D.; dos Santos Seckler, H.; DeHart, C. J.; Weisbrod, C. R.; Durbin, K. R.; Greer, J. B.; Early, B. P.; Fellers, R. T.; Zabrouskov, V.; Thomas, P. M.; Compton, P. D.; Kelleher, N. L. Thorough Performance Evaluation of 213 Nm Ultraviolet Photodissociation for Top-down Proteomics*. *Mol. Cell. Proteomics* **2020**, *19* (2), 405–420. https://doi.org/10.1074/mcp.TIR119.001638.
(50) Brodbelt, J. S.; Morrison, L. J.; Santos, I. Ultraviolet Photodissociation Mass Spectrometry for Analysis of Biological Molecules. *Chem. Rev.* **2019**, *120* (7), 3328–3380. https://doi.org/10.1021/ACS.CHEMREV.9B00440.
(51) Macias, L. A.; Santos, I. C.; Brodbelt, J. S. Ion Activation Methods for Peptides and Proteins. *Anal. Chem.* **2019**, *92* (1), 227–251. https://doi.org/10.1021/ACS.ANALCHEM.9B04859.
(52) Riley, N. M.; Westphall, M. S.; Hebert, A. S.; Coon, J. J. Implementation of Activated Ion Electron Transfer Dissociation on a Quadrupole-Orbitrap-Linear Ion Trap Hybrid Mass Spectrometer. *Anal. Chem.* **2017**, *89* (12), 6358–6366. https://doi.org/10.1021/acs.analchem.7b00213.
(53) Helms, A.; Escobar, E. E.; Vainauskas, S.; Taron, C. H.; Brodbelt, J. S. Ultraviolet Photodissociation Permits Comprehensive Characterization of O-Glycopeptides Cleaved with O-Glycoprotease IMPa. *Anal. Chem.* **2023**, *95* (24), 9280–9287. https://doi.org/10.1021/acs.analchem.3c01111.
(54) Escobar, E. E.; King, D. T.; Serrano-Negrón, J. E.; Alteen, M. G.; Vocadlo, D. J.; Brodbelt, J. S. Precision Mapping of O-Linked N -Acetylglucosamine Sites in Proteins Using Ultraviolet Photodissociation Mass Spectrometry. *J. Am. Chem. Soc.* **2020**, *142*, 11569–11577. https://doi.org/10.1021/jacs.0c04710.
(55) Hoffmann, M.; Pioch, M.; Pralow, A.; Hennig, R.; Kottler, R.; Reichl, U.; Rapp, E. The Fine Art of Destruction: A Guide to In-Depth Glycoproteomic Analyses—Exploiting the Diagnostic Potential of Fragment Ions. *Proteomics* **2018**, *18* (24), 1800282. https://doi.org/10.1002/pmic.201800282.

(56) Hevér, H.; Nagy, K.; Xue, A.; Sugár, S.; Komka, K.; Vékey, K.; Drahos, L.; Révész, Á. Diversity Matters: Optimal Collision Energies for Tandem Mass Spectrometric Analysis of a Large Set of N-Glycopeptides. *J. Proteome Res.* **2022**, *21* (11), 2743–2753. https://doi.org/10.1021/acs.jproteome.2c00519.
(57) Yang, H.; Yang, C.; Sun, T. Characterization of Glycopeptides Using a Stepped Higher-Energy C-Trap Dissociation Approach on a Hybrid Quadrupole Orbitrap. *Rapid Commun. Mass Spectrom.* **2018**, *32* (16), 1353–1362. https://doi.org/10.1002/rcm.8191.
(58) Liu, M.-Q.; Zeng, W.-F.; Fang, P.; Cao, W.-Q.; Liu, C.; Yan, G.-Q.; Zhang, Y.; Peng, C.; Wu, J.-Q.; Zhang, X.-J.; Tu, H.-J.; Chi, H.; Sun, R.-X.; Cao, Y.; Dong, M.-Q.; Jiang, B.-Y.; Huang, J.-M.; Shen, H.-L.; Wong, C. C. L.; He, S.-M.; Yang, P.-Y. pGlyco 2.0 Enables Precision N-Glycoproteomics with Comprehensive Quality Control and One-Step Mass Spectrometry for Intact Glycopeptide Identification. *Nat. Commun.* **2017**, *8* (1), 438. https://doi.org/10.1038/s41467-017-00535-2.
(59) Riley, N. M.; Malaker, S. A.; Driessen, M. D.; Bertozzi, C. R. Optimal Dissociation Methods Differ for *N* - and *O* -Glycopeptides. *J. Proteome Res.* **2020**, *19* (8), 3286–3301. https://doi.org/10.1021/acs.jproteome.0c00218.
(60) Pap, A.; Klement, E.; Hunyadi-Gulyas, E.; Darula, Z.; Medzihradszky, K. F. Status Report on the High-Throughput Characterization of Complex Intact O-Glycopeptide Mixtures. *J. Am. Soc. Mass Spectrom.* **2018**, *29* (6), 1210–1220. https://doi.org/10.1007/s13361-018-1945-7.
(61) Darula, Z.; Pap, Á.; Medzihradszky, K. F. Extended Sialylated O-Glycan Repertoire of Human Urinary Glycoproteins Discovered and Characterized Using Electron-Transfer/Higher-Energy Collision Dissociation. *J. Proteome Res.* **2019**, *18* (1), 280–291. https://doi.org/10.1021/acs.jproteome.8b00587.
(62) Riley, N. M.; Malaker, S. A.; Bertozzi, C. R. Electron-Based Dissociation Is Needed for O-Glycopeptides Derived from OpeRATOR Proteolysis. *Anal. Chem.* **2020**, *92* (22), 14878–14884. https://doi.org/10.1021/acs.analchem.0c02950.
(63) Singh, C.; Zampronio, C. G.; Creese, A. J.; Cooper, H. J. Higher Energy Collision Dissociation (HCD) Product Ion-Triggered Electron Transfer Dissociation (ETD) Mass Spectrometry for the Analysis of N-Linked Glycoproteins. *J. Proteome Res.* **2012**, *11* (9), 4517–4525. https://doi.org/10.1021/pr300257c.
(64) Saba, J.; Dutta, S.; Hemenway, E.; Viner, R. Increasing the Productivity of Glycopeptides Analysis by Using Higher-Energy Collision Dissociation-Accurate Mass-Product-Dependent Electron Transfer Dissociation. *Int. J. Proteomics* **2012**, *2012*, 1–7. https://doi.org/10.1155/2012/560391.
(65) Wu, S. W.; Pu, T. H.; Viner, R.; Khoo, K. H. Novel LC-MS2 Product Dependent Parallel Data Acquisition Function and Data Analysis Workflow for Sequencing and Identification of Intact Glycopeptides. *Anal. Chem.* **2014**, *86* (11), 5478–5486. https://doi.org/10.1021/ac500945m.
(66) Zhao, P.; Viner, R.; Teo, C. F.; Boons, G. J.; Horn, D.; Wells, L. Combining High-Energy C-Trap Dissociation and Electron Transfer Dissociation for Protein O-GlcNAc Modification Site Assignment. *J. Proteome Res.* **2011**, *10* (9), 4088–4104. https://doi.org/10.1021/pr2002726.
(67) Riley, N. M.; Coon, J. J. The Role of Electron Transfer Dissociation in Modern Proteomics. *Anal. Chem.* **2018**, *90* (1), 40–64. https://doi.org/10.1021/acs.analchem.7b04810.
(68) He, Y.; Shishkova, E.; Peters-Clarke, T. M.; Brademan, D. R.; Westphall, M. S.; Bergen, D.; Huang, J.; Huguet, R.; Senko, M. W.; Zabrouskov, V.; McAlister, G. C.; Coon, J. J. Evaluation of the Orbitrap Ascend Tribrid Mass Spectrometer for Shotgun Proteomics. *Anal. Chem.* **2023**, *95* (28), 10655–10663. https://doi.org/10.1021/acs.analchem.3c01155.

(69) Lee, L. Y.; Moh, E. S. X.; Parker, B. L.; Bern, M.; Packer, N. H.; Thaysen-Andersen, M. Toward Automated N-Glycopeptide Identification in Glycoproteomics. *J. Proteome Res.* **2016**, *15* (10), 3904–3915. https://doi.org/10.1021/acs.jproteome.6b00438.
(70) Zougman, A.; Selby, P. J.; Banks, R. E. Suspension Trapping (STrap) Sample Preparation Method for Bottom-up Proteomics Analysis. *PROTEOMICS* **2014**, *14* (9), 1006–1000. https://doi.org/10.1002/pmic.201300553.
(71) Rose, C. M.; Rush, M. J. P.; Riley, N. M.; Merrill, A. E.; Kwiecien, N. W.; Holden, D. D.; Mullen, C.; Westphall, M. S.; Coon, J. J. A Calibration Routine for Efficient ETD in Large-Scale Proteomics. *J. Am. Soc. Mass Spectrom.* **2015**, *26* (11), 1848–1857. https://doi.org/10.1007/s13361-015-1183-1.
(72) Lu, L.; Riley, N. M.; Shortreed, M. R.; Bertozzi, C. R.; Smith, L. M. O-Pair Search with MetaMorpheus for O-Glycopeptide Characterization. *Nat. Methods* **2020**, *17* (11), 1133–1138. https://doi.org/10.1038/s41592-020-00985-5.
(73) Riley, N.; Bertozzi, C. Deciphering O-Glycoprotease Substrate Preferences with O-Pair Search. *Mol. Omics* **2022**, 10.1039/D2MO00244B. https://doi.org/10.1039/D2MO00244B.
(74) Bern, M.; Kil, Y. J.; Becker, C. Byonic: Advanced Peptide and Protein Identification Software. *Curr. Protoc. Bioinforma. Ed. Board Andreas Baxevanis Al* **2012**, *Chapter 13*, Unit13.20. https://doi.org/10.1002/0471250953.bi1320s40.
(75) Roushan, A.; Wilson, G. M.; Kletter, D.; Sen, K. I.; Tang, W.; Kil, Y. J.; Carlson, E.; Bern, M. Peak Filtering, Peak Annotation, and Wildcard Search for Glycoproteomics. *Mol. Cell. Proteomics* **2021**, *20*, 100011. https://doi.org/10.1074/MCP.RA120.002260.
(76) Pino, L. K.; Searle, B. C.; Bollinger, J. G.; Nunn, B.; MacLean, B.; MacCoss, M. J. The Skyline Ecosystem: Informatics for Quantitative Mass Spectrometry Proteomics. *Mass Spectrom. Rev.* **2020**, *39* (3), 229–244. https://doi.org/10.1002/mas.21540.
(77) Perez-Riverol, Y.; Bai, J.; Bandla, C.; García-Seisdedos, D.; Hewapathirana, S.; Kamatchinathan, S.; Kundu, D. J.; Prakash, A.; Frericks-Zipper, A.; Eisenacher, M.; Walzer, M.; Wang, S.; Brazma, A.; Vizcaíno, J. A. The PRIDE Database Resources in 2022: A Hub for Mass Spectrometry-Based Proteomics Evidences. *Nucleic Acids Res.* **2021**, *50* (D1), D543. https://doi.org/10.1093/nar/gkab1038.
(78) Yu, Q.; Wang, B.; Chen, Z.; Urabe, G.; Glover, M. S.; Shi, X.; Guo, L. W.; Kent, K. C.; Li, L. Electron-Transfer/Higher-Energy Collision Dissociation (EThcD)-Enabled Intact Glycopeptide/Glycoproteome Characterization. *J. Am. Soc. Mass Spectrom.* **2017**, *28* (9), 1751–1764. https://doi.org/10.1007/s13361-017-1701-4.
(79) Riley, N. M.; Hebert, A. S.; Westphall, M. S.; Coon, J. J. Capturing Site-Specific Heterogeneity with Large-Scale N-Glycoproteome Analysis. *Nat. Commun.* **2019**, *10* (1), 1311. https://doi.org/10.1038/s41467-019-09222-w.
(80) Reiding, K. R.; Bondt, A.; Franc, V.; Heck, A. J. R. The Benefits of Hybrid Fragmentation Methods for Glycoproteomics. *TrAC - Trends Anal. Chem.* **2018**, *108*, 10.1016/j.trac.2018.09.007. https://doi.org/10.1016/j.trac.2018.09.007.
(81) Compton, P. D.; Strukl, J. V.; Bai, D. L.; Shabanowitz, J.; Hunt, D. F. Optimization of Electron Transfer Dissociation via Informed Selection of Reagents and Operating Parameters. *Anal. Chem.* **2012**, *84* (3), 1781–1785. https://doi.org/10.1021/ac202807h.
(82) Frese, C. K.; Altelaar, A. F. M.; van den Toorn, H.; Nolting, D.; Griep-Raming, J.; Heck, A. J. R.; Mohammed, S. Toward Full Peptide Sequence Coverage by Dual Fragmentation Combining Electron-Transfer and Higher-Energy Collision Dissociation Tandem Mass Spectrometry. *Anal. Chem.* **2012**, *84* (22), 9668–9673. https://doi.org/10.1021/ac3025366.
(83) Good, D. M.; Wirtala, M.; McAlister, G. C.; Coon, J. J. Performance Characteristics of Electron Transfer Dissociation Mass Spectrometry. *Mol. Cell. Proteomics MCP* **2007**, *6* (11), 1942–1951. https://doi.org/10.1074/mcp.M700073-MCP200.

(84) Liu, J.; McLuckey, S. A. Electron Transfer Dissociation: Effects of Cation Charge State on Product Partitioning in Ion/Ion Electron Transfer to Multiply Protonated Polypeptides. *Int. J. Mass Spectrom.* **2012**, *330–332*, 174–181. https://doi.org/10.1016/j.ijms.2012.07.013.
(85) Vainauskas, S.; Guntz, H.; McLeod, E.; McClung, C.; Ruse, C.; Shi, X.; Taron, C. H. A Broad-Specificity O-Glycoprotease That Enables Improved Analysis of Glycoproteins and Glycopeptides Containing Intact Complex O-Glycans. *Anal. Chem.* **2022**, *94* (2), 1060–1069. https://doi.org/10.1021/acs.analchem.1c04055.
(86) Shaffer, C. J.; Marek, A.; Pepin, R.; Slovakova, K.; Turecek, F. Combining UV Photodissociation with Electron Transfer for Peptide Structure Analysis. *J. Mass Spectrom.* **2015**, *50* (3), 470–475. https://doi.org/10.1002/jms.3551.
(87) McLuckey, S. A.; Stephenson, J. L. Ion/Ion Chemistry of High-Mass Multiply Charged Ions. *Mass Spectrom. Rev.* **1998**, *17* (6), 369–407. https://doi.org/10.1002/(SICI)1098-2787(1998)17:6<369::AID-MAS1>3.0.CO;2-J.
(88) Swaney, D. L.; McAlister, G. C.; Wirtala, M.; Schwartz, J. C.; Syka, J. E. P.; Coon, J. J. Supplemental Activation Method for High-Efficiency Electron-Transfer Dissociation of Doubly Protonated Peptide Precursors. *Anal. Chem.* **2007**, *79* (2), 477–485. https://doi.org/10.1021/ac061457f.
(89) Calle, B.; Bineva-Todd, G.; Marchesi, A.; Flynn, H.; Ghirardello, M.; Tastan, O. Y.; Roustan, C.; Choi, J.; Galan, M. C.; Schumann, B.; Malaker, S. A. Benefits of Chemical Sugar Modifications Introduced by Click Chemistry for Glycoproteomic Analyses. *J. Am. Soc. Mass Spectrom.* **2021**, *32* (9), 2366–2375. https://doi.org/10.1021/JASMS.1C00084/SUPPL_FILE/JS1C00084_SI_001.PDF.
(90) Polasky, D. A.; Yu, F.; Teo, G. C.; Nesvizhskii, A. I. Fast and Comprehensive N- and O-Glycoproteomics Analysis with MSFragger-Glyco. *Nat. Methods 2020 1711* **2020**, *17* (11), 1125–1132. https://doi.org/10.1038/s41592-020-0967-9.

FIGURES

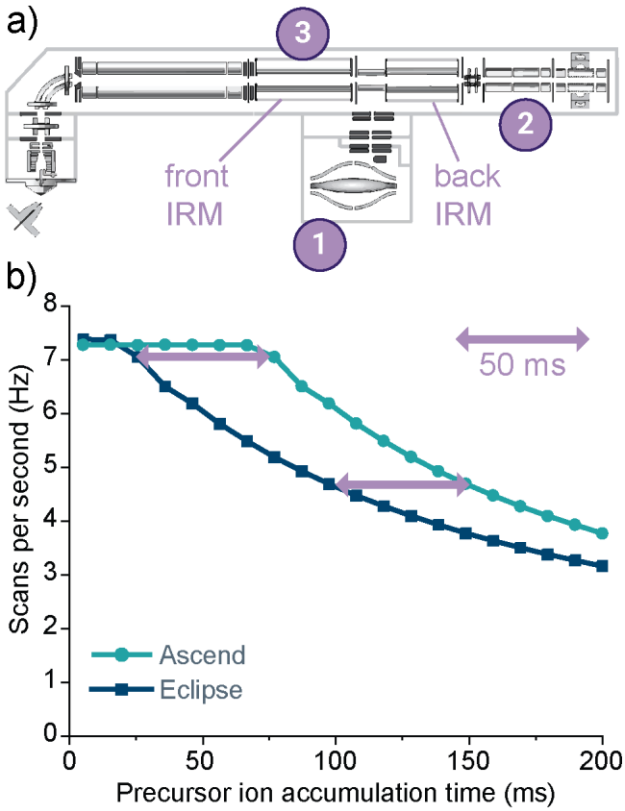

Figure 1. Architecture changes to the Orbitrap Tribrid MS platform provide more parallelization of scan functions. a) The addition of a second ion routing multipole (IRM) before the C-trap, i.e., the front IRM, on the Orbitrap Ascend MS allows simultaneous manipulation of three ion populations: 1) mass analysis in the Orbitrap, 2) tandem MS functions in the linear ion trap and back IRM, and 3) accumulation and/or beam-type collisional activation of precursor ions in the front IRM. **b)** When controlling for scan function overhead times like Orbitrap detection time (128 ms for a 60k resolution scan), a 50 ms ion-ion reaction time for ETD, and a 10 ms ETD reagent anion accumulation time, the dual IRM Tribrid architecture on the Orbitrap Ascend MS provides ~50 ms of additional precursor ion accumulation time without sacrificing scan acquisition speeds relative to the single IRM architecture on the Orbitrap Eclipse MS.

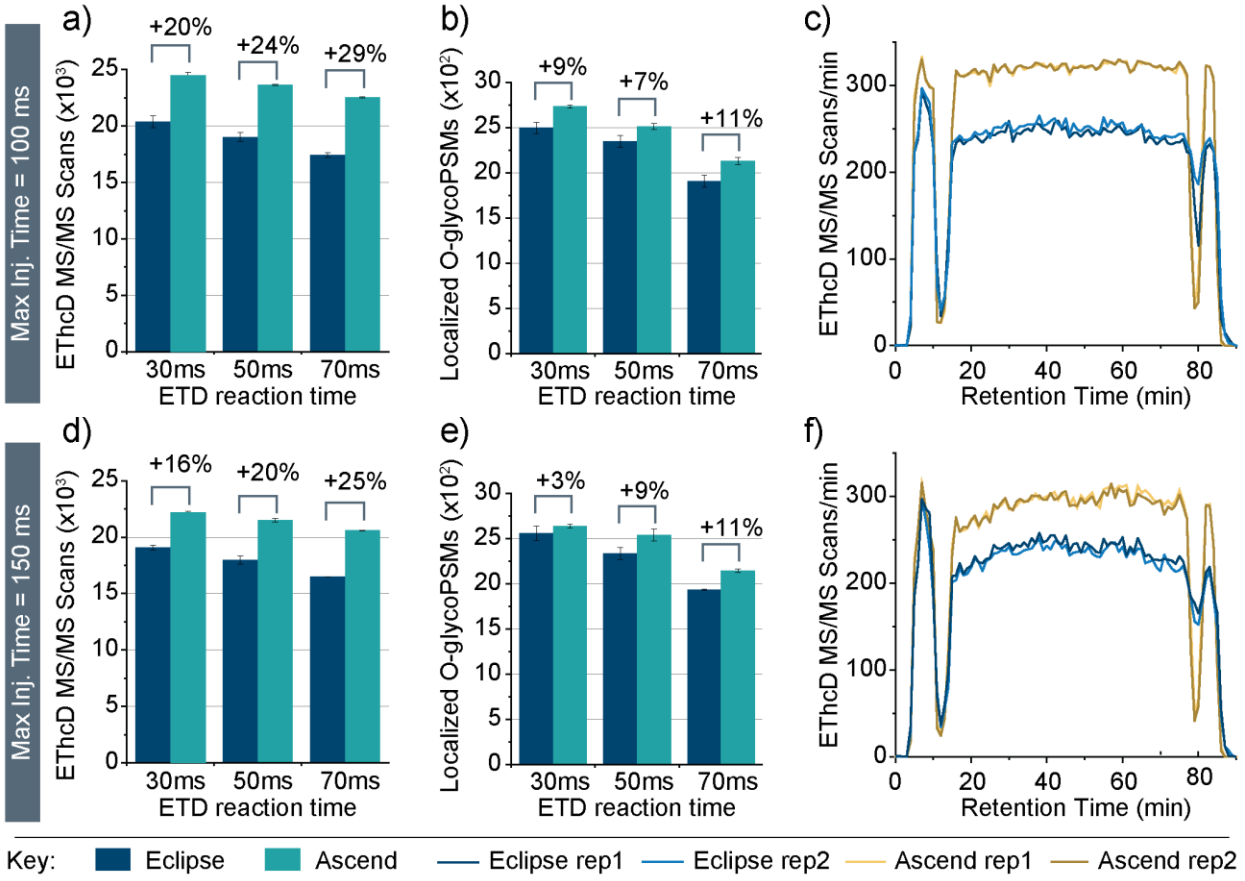

Figure 2. The dual IRM architecture of the Orbitrap Ascend MS generates more EThcD MS/MS scans and localized O-glycopeptides. An O-glycopeptide mixture was measured in technical duplicates on the Orbitrap Ascend MS and the Orbitrap Eclipse MS using EThcD fragmentation with 30, 50, and 70 ms ion-ion reaction times. Supplemental HCD activation was kept at 25% NCE. The top row shows data for methods using a 100 ms maximum precursor ion injection time (panels **a-c**), and the bottom row shows data for a 150 ms maximum injection time (panels **d-f**). The number of EThcD MS/MS scans (**a,d**) and O-glycopeptides (**b,e**) are compared for the Eclipse (navy) and Ascend (teal), with the percentage gain provided by the Ascend shown for each condition. All data here represent technical duplicate injections. Bar heights show replicate averages, and error bars show the individual replicates. When plotting scans per minute across 90-minute LC-MS/MS acquisitions using 50 ms reaction times (**c,f**), the Ascend was able to consistently acquire scans of about 80 more scans per minute during the time when the sample was eluting (starting at ~18 min).

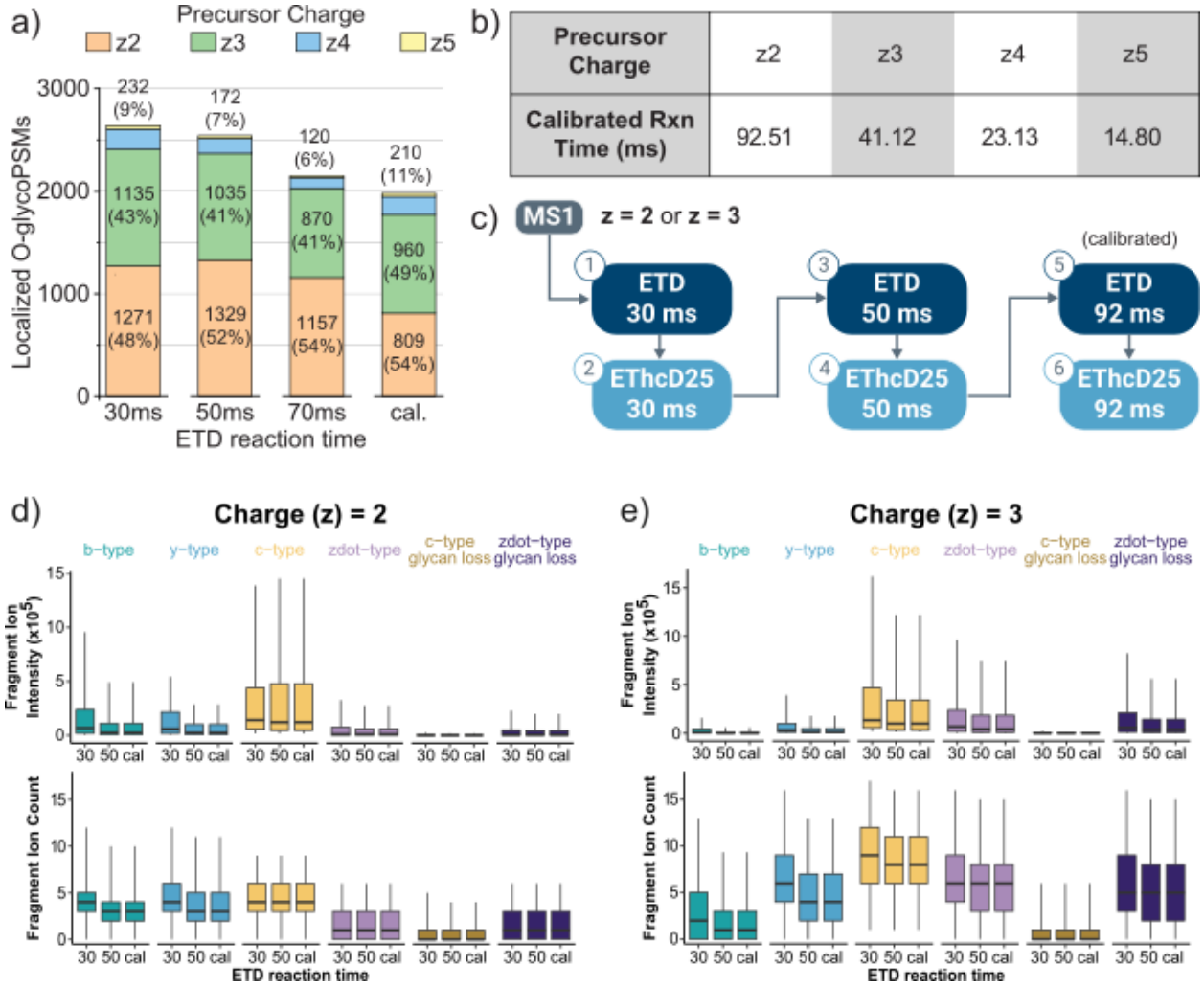

Figure 3. Comparing static and calibrated ion-ion reaction times for O-glycopeptide EThcD spectra. a) Localized O-glycopeptide spectral matches, broken down by precursor ion charge state, from Ascend data using 30 ms, 50 ms, 70 ms, or calibrated ion-ion reaction times. Numbers and percentages from each charge state are provided, with z = 4 and z = 5 presented in aggregate. **b)** A table showing calibrated reaction times that were automatically determined on the Ascend. **c)** Method design to investigate the influence of ion-ion reaction time on fragment ion production. Each precursor is selected for six subsequent MS/MS scans. In panels **d** and **e**, distributions of fragment ion intensity (top) and count (bottom) are shown for localized O-glycopeptides identified from EThcD spectra with varying ion-ion reaction times for z = 2 and z = 3 precursor ions, respectively. Fragment ion types are separated out by type, including b-, y-, c-, z•-, c-glycan loss fragments, and z•-glycan loss fragments. Boxes represent first and third quartiles, and the median is shown with a black bar. Whiskers show 10-90 percentiles.

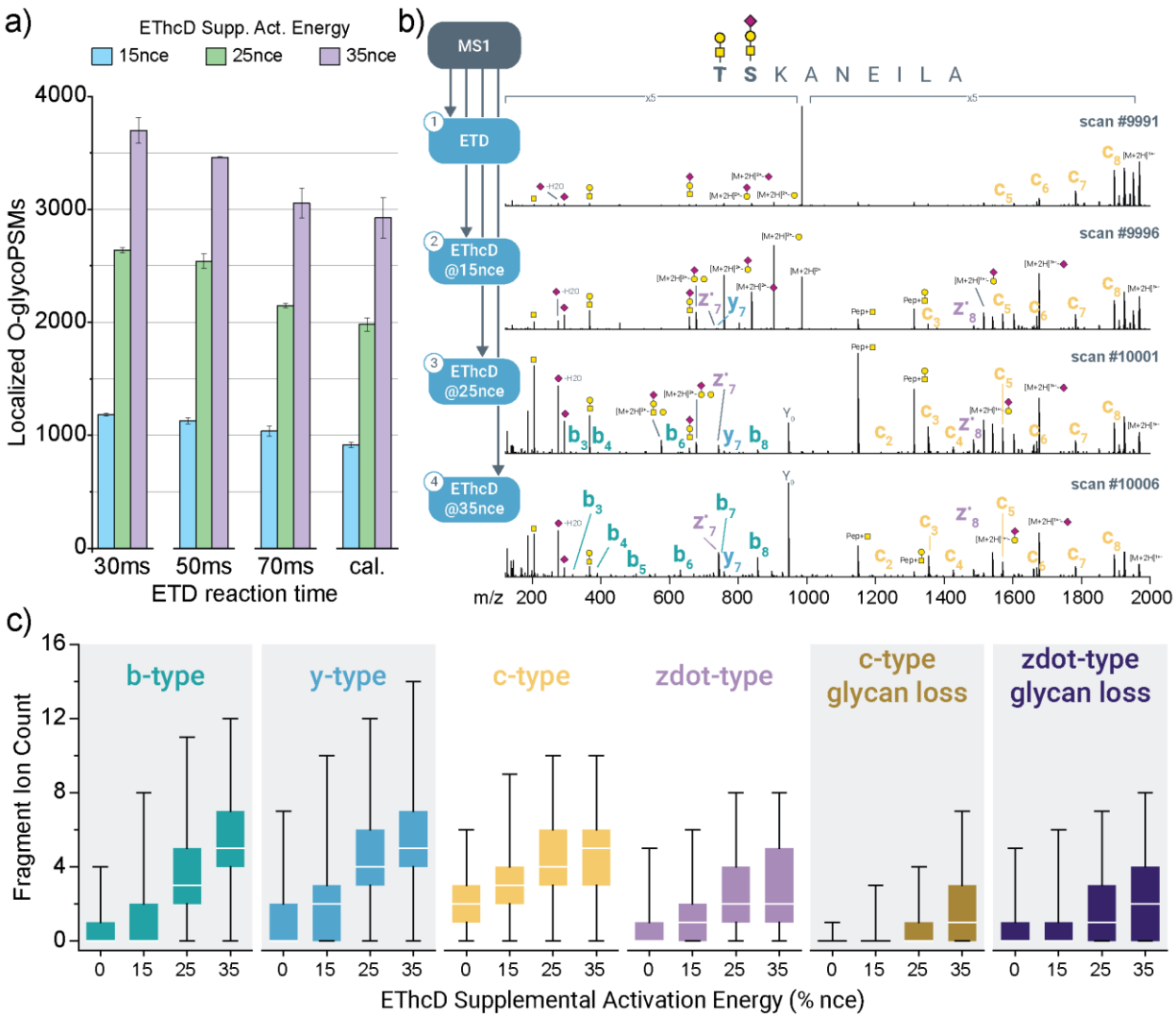

Figure 4. Effects of EThcD supplemental activation energy on O-glycopeptide identifications and fragment ion generation. a) O-glycopeptide spectral matches using various ion-ion reaction times and EThcD supplemental activation energies of 15%, 25%, or 35% NCE. **b)** Method design used to collect O-glycopeptide spectra at different collision energies on the Orbitrap Ascend. An example doubly glycosylated O-glycopeptide shows annotated spectra collected using this data-dependent acquisition scheme that acquired four MS/MS spectra per precursor ion. **c)** The distribution of fragment ion counts, delineated by fragment ion types, for localized O-glycopeptide identifications each of the EThcD supplemental collision energies used. All scans used a 50 ms ETD reaction time. Boxes in box plots represent first and third quartiles, and the median is shown with a black bar. Whiskers show 10-90 percentiles. The gray boxes denote “unmodified” fragment ion types, i.e., those that do not retain glycan modifications.

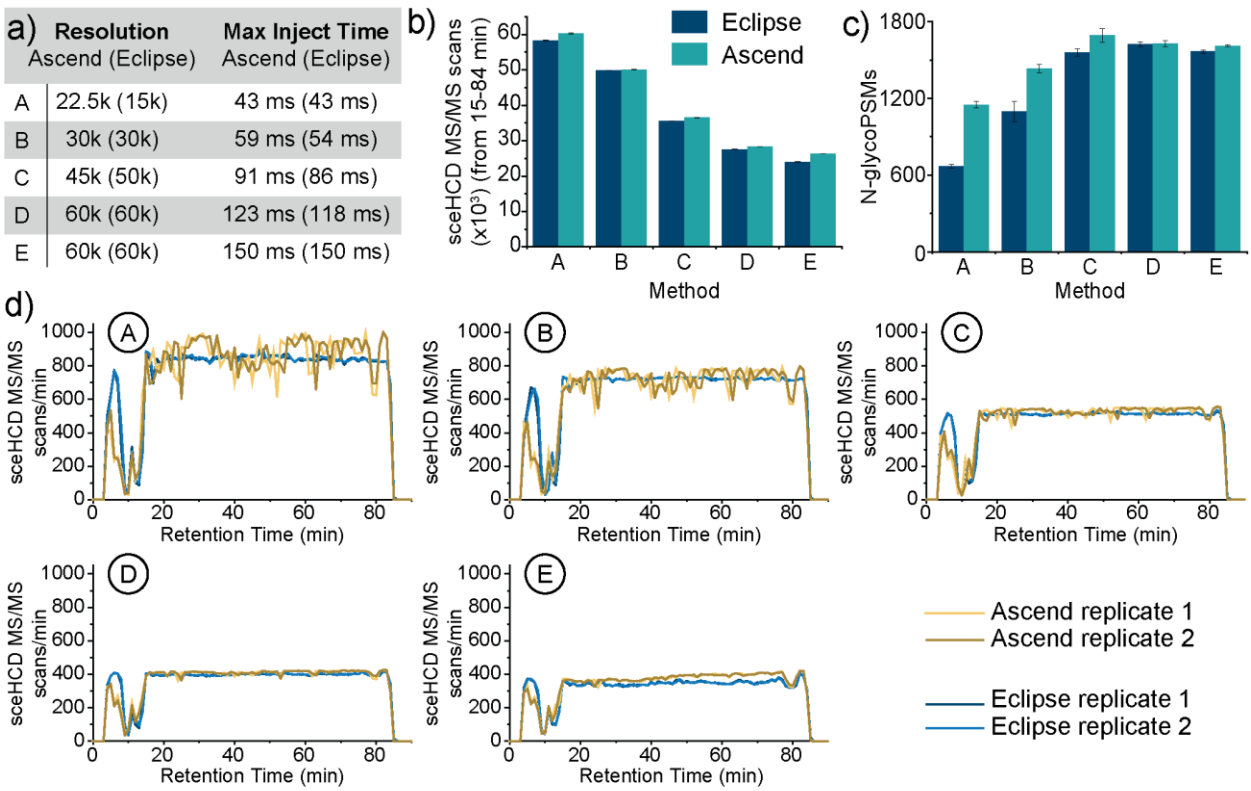

Figure 5. N-glycopeptide identifications with sceHCD methods on the Orbitrap Ascend and Orbitrap Eclipse. a) Five different sceHCD methods were tested for N-glycopeptide identification, where Orbitrap resolution and corresponding maximum parallizeable injection time (and by extension, scan acquisition speeds) were varied. The number of sceHCD MS/MS scans (**b**) and N-glycopeptides (**c**) are compared for the Eclipse (navy) and Ascend (teal). All data here represent technical duplicate injections. Bar heights show replicate averages and error bars show the individual replicates. **d)** Comparisons of sceHCD MS/MS scans per minute for the Ascend and the Eclipse across 90-minute LC-MS/MS acquisitions using various resolution and maximum precursor injection time settings.

FOR TOC ONLY